PERK inhibition in zebrafish mimics human Wolcott-Rallison syndrome phenotypes

Liliana M. Almeida[1,2], Leonor Pereira Lima[1,2], Nuno A. S. Oliveira[1,2], Rui F. O. Silva[1,2], Bruno Sousa[1,2], José Bessa[3,4], Brígida R. Pinho[1,2], Jorge M. A. Oliveira[1,2]

[1]UCIBIO-REQUIMTE – Applied Molecular Biosciences Unit, mitochondria and Neurobiology lab, Faculty of Pharmacy, University of Porto, Portugal

[2]Associate Laboratory i4HB - Institute for Health and Bioeconomy, mitochondria and Neurobiology lab, Faculty of Pharmacy, University of Porto, Portugal

[3] Instituto de Biologia Molecular e Celular (IBMC), Universidade do Porto, Porto, 4200-135, Portugal

[4] Instituto de Investigação e Inovação em Saúde (i3S), Universidade do Porto, Porto, 4200-135, Portugal

Corresponding author:
Jorge M. A. Oliveira (jorgemao@ff.up.pt)
Departamento de Ciências do Medicamento, Laboratório de Farmacologia, Faculdade de Farmácia, Universidade do Porto
Rua de Jorge Viterbo Ferreira, 228, 4050-313 Porto, Portugal
Tel. +351 220428610

Abstract (100 – 250 words)

Wolcott-Rallison Syndrome (WRS) is the most common cause of permanent neonatal diabetes mellitus among consanguineous families. The diabetes associated with WRS is non-autoimmune, insulin-requiring and associated with skeletal dysplasia and growth retardation. The therapeutic options for WRS patients rely on permanent insulin pumping or on invasive transplants of liver and pancreas. WRS has a well identified genetic cause: loss-of-function mutations in the gene coding for an endoplasmic reticulum kinase named PERK (protein kinase R-like ER kinase). Currently, WRS research is facilitated by cellular and rodent models with PERK ablation. While these models have unique strengths, cellular models incompletely replicate the organ/system-level complexity of WRS, and rodents have limited scalability for efficiently screening potential therapeutics. To address these challenges, we developed a new in vivo model of WRS by pharmacologically inhibiting PERK in zebrafish. This small vertebrate displays high fecundity, rapid development of organ systems and is amenable to highly efficient in vivo drug testing. PERK inhibition in zebrafish produced typical WRS phenotypes such as glucose dysregulation, skeletal defects, and impaired development. PERK inhibition in zebrafish also produced broad-spectrum WRS phenotypes such as impaired neuromuscular function, compromised cardiac function and muscular integrity. These results show that zebrafish holds potential as a versatile model to study WRS mechanisms and contribute to the identification of promising therapeutic options for WRS.

Keywords: rare disease; diabetes, embryonic development; animal disease model; drug testing; transgenic

1. Introduction

Wolcott-Rallison Syndrome (WRS) is a rare (ORPHA:1667) autosomal recessive disorder caused by loss-of-function mutations in the *EIF2AK3* gene encoding eukaryotic translation initiation factor 2α (eIF2α) kinase 3, also called protein kinase RNA-like endoplasmic reticulum kinase (PERK) (2000.Delepine.NatGen; 2010.Julier.OrphJRareDis). PERK is an endoplasmic reticulum (ER) membrane kinase whose main function is to respond to alterations in ER protein homeostasis (proteostasis) by activating the integrated stress response (ISR). ISR either recovers proteostasis or induces the expression of pro-apoptotic factors, therefore determining cell fate (2022.Almeida.BiolRev).

PERK is ubiquitously expressed throughout the body, being particularly abundant in bones and pancreas. This relative abundance of PERK likely explains WRS symptomatology, whose hallmarks include skeletal dysplasia and neonatal diabetes mellitus (2010.Julier.OrphJRareDis)., Despite being considered a rare disease (prevalence < 1/1 000 000 cases, ORPHANET data), WRS is the most common cause of permanent neonatal diabetes mellitus in consanguineous families (2010.Julier.OrphJRareDis). Broad-spectrum WRS symptoms include motor neuropathy, intellectual deficit, early neurodegeneration and cardiac malformations. The widespread distribution of PERK and the existence of several loss-of-function mutations that prematurely terminate PERK translation, totally or partially abolishing it's kinase activity contribute to the presence of brad spectrum WRS symptoms (2010.Julier.OrphJRareDis, 2004.Senée.Diabetes, 2015.Bruch.JNeuropatholExpNeurol).

The prognosis of WRS patients is usually poor and death occurs at a young age (< 35 years old) from multiple organ failure with predominant liver and renal dysfunction, hepatic failure and also encephalopathy (2010.Julier.OrphJRareDis). Existing therapies include blood glucose control with insulin pumping and transplant of liver pancreas and kidney (2015.Tzakis.AmJTransplant). The scarcity of non-invasive and more effective therapeutic

options for WRS patients highlights the need for further therapeutic investigation where efficient WRS models are vital. The currently available WRS models are mice with loss-of-function mutations of PERK that exhibit the WRS hallmarks – neonatal diabetes and skeletal dysplasia (2001.Harding.MolCell; 2002.Zhang.MolCellBiol) – and also the broad-spectrum phenotypes – cardiac, muscle and cognitive abnormalities (2021.Shimizu.SciRep, 2019.Gallot.FASEBJ, 2012.Trinh.CellRep). However, these rodent-based WRS models are unsuitable for exploratory studies of new therapeutics in larger scale. Further, despite the phylogenetic proximity to humans, the development of key structures for WRS pathophysiology like the pancreas occurs differently in humans and in rodents – insulin secreting β cells are the first cells to develop in zebrafish and humans, while in mouse they develop only after glucagon-secreting α cells (2017.Prince.CurTopDevBiol).

Zebrafish, have become increasingly interesting disease models in the scientific community because they present several advantages: high fecundity, external fertilization, and rapid (48-72h) complete organ formation. These advantages make zebrafish suitable for rapid, large-scale drug testing. Furthermore, zebrafish have a fully sequenced genome, are easy to manipulate genetically and present an elevated percentage of identity with humans, rendering them highly advantageous in studies of genetic diseases (2019.Teame.AnimFront; 2021.Choi.ExpMolMed), such as WRS.

In this article, we used a previously known PERK inhibitor, GSK2606414, in zebrafish embryos to test the feasibility of creating a zebrafish model of WRS that mimics both the hallmarks and broad-spectrum phenotypes.

2. Material and Methods

2.1 Drugs, solvents and solutions

GSK2606414 (Merck Millipore, 516535) was used to inhibit PERK (2012.Stockwell.PLoSOne). Stock drug solutions were prepared in anhydrous DMSO (Sigma, 276855). Tubocurarine hydrochloride pentahydrate (dTC, Sigma, t2379) solution was prepared in MilliQ water and used as a muscle relaxant. Prior to assays, stocks were diluted in embryo (E3) medium: 5 mM NaCl (Sigma, S9888), 0.17 mM KCl (Chem-Lab, cl00.1133.1000), 0.33 mM CaCl2•2H2O (Panreac, 131232.1211), 0.33 mM MgCl2•6H2O (Sigma, TA523733) and 0.0001% methylene blue (Sigma, M9140). Tricaine methanesulfonate (Sigma, E10521) was used as anesthetic at 0.02%. DMSO was always kept at safe concentrations (2021.Hoyberghs.FrontToxicol) up to 0.15%.

2.2 Zebrafish maintenance and husbandry

Adult AB strain zebrafish were supplied by the Interdisciplinary Centre of Marine and Environmental Research (CIIMAR, Portugal) and maintained in 45L tanks at 28 ± 1°C on a 14 h:10 h light:dark cycle and handled for egg production as we previously detailed (2022.Silva.Chemosphere, 2019.Pinho.FRBM). Briefly, adults (1:1, male:female) were placed in a 0.7 L breeding tank with circulating water in contact with the main tank on the day before egg collection. Ninety minutes after starting the light period, eggs were collected and washed. This time point was recorded as 0 h post fertilization (hpf).

125 **2.3 Embryo maintenance and drug treatments**

126

127 Embryos were randomly distributed in 24-well plates (5 embryos/well; 0.5 mL E3/well) and
128 kept at 28 ± 1°C on a 14 h:10 h light: dark cycle throughout the assay. Embryos were
129 continuously exposed to GSK2606414 or solvent (DMSO) from 4 to 76 hpf and solutions were
130 renewed daily (2022.Silva.Chemosphere,). All drug concentrations were assayed in duplicate
131 wells (5 + 5 eggs), in at least three independent experiments (≥ 30 eggs) (2013.Pinho.BJP).
132 dTC was incubated for 10 minutes before assays endpoint in 5 embryos, in at least three
133 independent experiments (≥ 15 embryos).

134

135 **2.4 Brightfield microscopy**

136 For brightfield microscopy, a stereomicroscope (Stemi DV4, Zeiss, Göttinger, Germany) or an
137 inverted microscope (Eclipse TE300, Nikon, Tokyo, Japan) were used. The inverted
138 microscope was attached to a motorized stage (ProScan, Prior) and a CCD camera (ORCA-
139 ER, Hamamatsu), all controlled by the open-source software Micro-Manager (v. 2.0;
140 https://micro-manager.org). This Nikon-Prior-Hamamatsu (NPH) imaging system was used to
141 perform the following brightfield imaging protocols:

142 **2.4.1 Monitoring zebrafish development**

143 At regular time points (28, 52 and 76 hpf) embryos were scored as normal, abnormal
144 or dead; hatched (ruptured chorion and free tail movement) or unhatched. Embryos
145 were classified as dead if lacking one of the following: somite formation, tail
146 detachment or heartbeat, as according to OECD guideline 236 (OECD, 2013). Normal
147 development was as previously described (1995.Kimmel.DevDyn). Abnormalities
148 were scored as cardiac and skeletal (further into scoliosis, lordosis or kyphosis).

149 **2.4.2 Morphometric analysis**

150 Brightfield images were used for morphometric analysis of head-tail angle and body
151 length of zebrafish. Body length was measured from the tip of the zebrafish head
152 (between the eyes) to the end of the tail (2019.Martinez.STotEn). Trunk-tail angle was
153 measured with the angle tool of ImageJ as the angle formed by notochord rostral vs
154 caudal do the anus (Figure 3 B). Both parameters (length and angle) were quantified by
155 a researcher blinded to experimental conditions.

156 **2.4.3 Heartbeat and atrio-ventricular coordination**

157 Heart rates were counted by microscopic visualization of at least two larvae per well (4
158 larvae per condition, per experiment), during 20 s, at 72-80 hpf (2013.Pinho.BJP).
159 Recordings of atrio-ventricular coordination were obtained by imaging live larvae for
160 90 seconds at 12 frames per second. After the experiments, the atrium and ventricle
161 were visually identified, and the recordings were obtained with "Plot Z-axis profile" on
162 ImageJ.

163 **2.4.4 Tail coilings**

164 Zebrafish spontaneous activity was assessed by monitoring tail coiling movements at
165 28 hpf in glass bottom 96-well plates. Each embryo was imaged for 3 minutes at a
166 frequency of 4.5 frames per second and 2x2 or 4x4 binning. After imaging, tail coilings
167 were counted by researchers blinded to experimental conditions
168 (2024.Oliveira.FreeRadBiolMed).

169 **2.4.5 Birefringence analysis**

170 For muscle birefringence analysis, 76 hpf larvae were anesthetized immobilized on a
171 glass surface, oriented laterally and illuminated with linearly polarized light (Screen-
172 Tech, ST-38). An orthogonal polarization filter was placed after the samples to block
173 directly transmitted light. Thus, only light whose polarization angle is affected by the
174 sample is collected by the NPH microscope. Pixel intensity in the trunk region was

175 measured by selecting the region of interest with ImageJ software by a researcher
176 blinded to experimental conditions.
177
178 **2.5 Touch-evoked escape response (TEER)**
179
180 At 76 hpf, at least two embryos per well (6 embryos per condition) were submitted to 10
181 alternated touches to the head and to the tail with a 10 µL pipette tip with a recovery time of
182 30 seconds (2016.Pinho.PharmRes). Data is presented as response rates in percentage of total
183 touches.
184
185 **2.6 Fluorescent labelling and microscopy of zebrafish**
186
187 At 73 hpf, larvae were incubated with a fluorescent glucose analogue - 600 µM 2-NBDglucose
188 (2-(7-Nitro-2,1,3-benzoxadiazol-4-yl)-D-glucosamine) (200 µL, Tebu-Bio, 10-1459)
189 (2013.Lee.ACSChemBiol; 2020.Wang.OrgBiomolChem); and a positive control for
190 neuromast labelling - Mitotracker Deep Red (1 µM, Invitrogen, M22426) for 3 hours in 96 well
191 plates (4 larvae/well) (2013.Lee.ACSChemBiol; 2020.Wang.OrgBiomolChem). At 76 hpf,
192 each larva was washed twice with E3 solution, anesthetized with 0.02% tricaine
193 methanesulfonate (Sigma, E10521) and imaged in a glass-bottom chamber. For imaging, we
194 used the NPH microscope with a monochromator (Polychrome II, Photonics). 2-NBDglucose
195 was excited at 475 nm and Mitotracker Deep Red at 650 nm for 1 second. Emissions were
196 collected using band pass filters (Chroma 69008 – ET – ECFP/EYFP/mCherry) with a 10 ×
197 objective. Images of the entire fish were stitched with the GNU image manipulation program
198 (The GIMP Development Team, 2019). Retrieved from https://www.gimp.org). The number
199 of labelled anterior and posterior neuromasts

200 (2017_Stengel_CompBiochemPhysiolCToxicolPharmacol) was counted and plotted by
201 researchers blinded to experimental conditions.
202
203 **2.7 Imaging of fluorescent transgenic zebrafish**
204 Double transgenic zebrafish larvae expressing GFP in insulin-producing cells and mCherry in
205 elastase producing-cells, Tg(*ins:GFP, ela:mCherry*), or expressing GFP in insulin-producing
206 cells and mCherry in somatostatin producing-cells, Tg(*ins:GFP, sst:mCherry*)
207 (2020.Eufrasio.Diabetes), were obtained from José Bessa's laboratory at the Institute for
208 Research and Innovation in Health (i3s, Porto, Portugal). Larvae were kept in 24-well plates (5
209 larvae/plate) with E3 media until the start of drug treatments (DMSO 0.15%, GSK2606414 3–
210 10 μM). We used two pharmacological approaches: 1) GSK2606414 exposure from 4 hpf
211 (before the principal islet of Langerhans is formed within the endocrine pancreas) to 28, 76 or
212 148 hpf; 2) GSK2606414 exposure from 76 hpf (when the principal islet is already formed) to
213 148 hpf (2009.Tiso.MolCelEndocrinol). Drug solutions were renewed daily. At the final time
214 point (28, 76 or 148 hpf) larvae were anesthetized by rapid cooling on ice and fixed in 4%
215 paraformaldehyde overnight. Larvae were imaged with the NPH inverted microscope. GFP
216 was excited at 488 nm and mCherry was excited at 575 nm. Emissions were collected using
217 band pass filters (Chroma 59022 – EGFP/mCherry) with a 20 × objective. The area of GFP- or
218 mCherry-labelled pancreas in each image was assessed with ImageJ software by a researcher
219 blinded to the treatment conditions.
220
221 **2.8 Western Blot**
222 24 to 27 larvae per condition were rinsed with ice-cold system water twice before being placed
223 in RIPA buffer (50 mM Tris (NZYTech, MB01601), 150 mM NaCl (Merck, S9888), 1 mM
224 EDTA (Sigma-Aldrich, E6758), 1% IGEPAL CA-630 (Sigma-Aldrich, I3021), 1% sodium

225 deoxycholate (Sigma-Aldrich, D6750), 0.1% sodium dodecyl sulfate (Sigma-Aldrich, L3771))
226 supplemented with a protease and phosphatase inhibitor cocktail (Thermo Scientific, 78440).
227 After 3 freeze-thaw cycles, samples were homogenized with Precellys Evolution (6800 rpm, 5
228 × 42 s with 37 s interval) and centrifuged at 12,000 × g (10 min, 4 °C). Supernatant protein
229 concentrations were quantified by the Bradford method. Protein extracts supplemented with
230 Bolt LDS sample buffer (Invitrogen, B0007) and Bolt sample reducing agent (Invitrogen,
231 B0009) were denatured at 95 ºC for 5 min. 30 to 40 µg of protein were loaded into 4–15%
232 Mini-PROTEAN® TGX™ Precast Protein Gels (Biorad, 4561084), electrophoresed between
233 125 and 200 V for 30 min and wet-transferred to PVDF membranes (Millipore, IPVH00010)
234 overnight (30 V, 4ºC). Membranes were then blocked (1 h, room temperature or overnight at
235 4ºC) with 5% bovine serum albumin (BSA, NZYTech, MB04602) in PBS with 0.05% Tween
236 20 (PBST) and then incubated with primary antibodies: anti-ATF4 (1:500, overnight,
237 Proteintech Cat# 10835-1-AP, RRID: AB_2058600); anti-CHOP (1:1000, overnight,
238 Proteintech Cat# 15204-1-AP, RRID:AB_2292610); anti-eIF2α (1:1000, overnight, Thermo
239 Fisher Scientific Cat# AHO0802, RRID: AB_2536316); anti-p-eIF2α (1:500, overnight,
240 Thermo Fisher Scientific Cat# MA5-15133, RRID:AB_10983400). After washing with PBST
241 for 15 min, membranes were incubated with respective horseradish peroxidase-conjugated
242 secondary antibodies for 1 h: anti-mouse (1:4000, 1 h, Thermo Fisher Scientific Cat# G-21040,
243 RRID: AB_2536527); anti-rabbit (1:4000, 1 h, Thermo Fisher Scientific Cat# G-21234,
244 RRID:AB_2536530). Detection was performed using a Chemiluminescent kit (Novex ECL,
245 Invitrogen, WP20005) and a ChemiDoc MP Imaging system (Bio-Rad). Membrane Coomassie
246 (Sigma-Aldrich, 27816) staining was used for loading control. Densitometric analyses were
247 performed with Image J (https://imagej.nih.gov/ij/). In each independent experiment, samples
248 from control and 10 µM GSK- treated larvae were run in the same gel.
249

250 **2.8 Bioinformatic analysis**

251 **2.8.1 Comparison of PERK orthologues**

252 Protein sequence data from zebrafish (*Danio rerio,* XP_005156642.2), human (*Homo*
253 *sapiens,* AAI26357.1), mouse (*Mus musculus,* AAH54809.1), fruit fly (*Drosophila*
254 *melanogaster,* AAF61200.1), and nematode (*Caenorhabditis elegans*, AAF61201.1)
255 were obtained from NCBI Protein (https://www.ncbi.nlm.nih.gov/protein/). The amino
256 acid sequence from the total human PERK protein and from its catalytic domain were
257 compared with its orthologue proteins from zebrafish, mouse, fruit fly, and nematode,
258 using the Protein BLAST tool (https://blast.ncbi.nlm.nih.gov/Blast.cgi). Additionally,
259 we determined the identity of the vital amino acids for GSK2606414 binding to the
260 catalytic site of PERK, by aligning the protein sequence from zebrafish and human.

261

262 **2.8.2 Zebrafish PERK 3D structure and molecular docking**

263 The predicted three-dimensional protein structures of zebrafish PERK (UniProt:
264 B8JI14) and human PERK (UniProt: Q9NZJ5) were obtained from AlphaFold Protein
265 Structure Database (2021.Jumper.Nature; 2022.Varadi.NucleicAcidsRes). To visualize
266 and align the three-dimensional structures of human PERK (PDB: 4g31), zebrafish
267 PERK (UniProt: B8JI14), and GSK2606414 (2021.Pettersen.ProteinSci) we used
268 UCSF ChimeraX developed by the Resource for Biocomputing, Visualization, and
269 Informatics at the University of California, San Francisco, with support from National
270 Institutes of Health R01-GM129325 and the Office of Cyber Infrastructure and
271 Computational Biology, National Institute of Allergy and Infectious Diseases
272 (2020_Pettersen_ProtSci). The human GSK2606414-bound PERK structure (PDB:
273 4g31) was used as a starting model and superimposition with zebrafish PERK was done
274 in UCSF ChimeraX, using the Matchmaker tool. To assess the structural similarity

275 between zebrafish and human PERK and infer about GSK2606414 binding efficiency,
276 we calculated the root-mean-square deviation (RMSD) in ChimeraX software for the
277 total protein and for the catalytic site of zebrafish PERK, and performed a
278 Ramachandran plot analysis in SWISS-MODEL online server for the total protein of
279 zebrafish PERK (2018.Waterhouse.NucleicAcidsRes).
280
281 **2.9 Statistical Analysis**
282
283 Data are shown as mean ± standard error of the mean (SEM) of the *n* specified in figure legends,
284 except for zebrafish survival data that are shown as Kaplan-Meier representations and result
285 from 5 independent breedings. The Mantel-Cox (Log-rank) test was used to assess differences
286 in larval survival curves upon different treatments. Student's *t*-test was used to evaluate the
287 effect of GSK2606414 treatment vs. control in the quantification of protein levels (western
288 blot), the area of different pancreatic structures and 2-NBDGlucose labelled neuromasts. One-
289 Way ANOVA with Dunnett's post-hoc test was used to assess effects between drug
290 concentrations. Two-way ANOVA was used to test for interactions and main effects of the
291 factors: treatment (GSK2606414 concentrations) vs. time of treatment (28, 52, 76 hpf). When
292 two-factor interactions were significant, multiple comparisons among groups were performed
293 with Sidak's post-hoc test. For all analyses, a *P* value under 0.05 was taken as statistically
294 significant. Data analyses were performed with Prism 6.0 (GraphPad).
295
296
297

298 **3. Results**

299

300 **3.1 The PERK-GSK2606414 binding site is conserved in humans and zebrafish**

301

302 To model WRS in zebrafish larvae we wanted to determine if zebrafish and human PERK
303 exhibit a high degree of similarity and if an inhibitor known to have *in vivo* activity in mice
304 would bind to zebrafish PERK. We chose GSK2606414 (hereafter designated as GSK; not to
305 be confused with glycogen synthase kinase) to inhibit PERK, for three reasons: 1) it is one of
306 the most commonly PERK inhibitor used in scientific research (2022.Almeida.BiolRev); 2) to
307 this date it is the only inhibitor with documented penetration of the blood-brain barrier in
308 animals (2013.Moreno.SciTranslMed); and 3) previous molecular modelling studies showed
309 the structure of GSK-bound PERK and revealed which amino acids in human PERK's catalytic
310 domain are vital for GSK binding (2012.Axten.JMedChem, 2020.Chintha.RSCAdvances). To
311 predict the effectiveness of using GSK in zebrafish, we used bioinformatic tools that quantified
312 the sequence identity of PERKs aminoacidic structure between humans and zebrafish.

313 Using the bioinformatic alignment tool BLASTP, we quantified the identity between
314 the PERK aminoacidic sequence in humans and nematodes (*Caenorhabditis elegans*), fruit-
315 flies (*Drosophila melanogaster*), zebrafish (*Danio rerio*) and mouse (*Mus musculus)* (Figure 1
316 A). As expected, due to phylogenetic proximity, the percentage of identity between human and
317 zebrafish PERK is lower than between human and mouse but higher than between human and
318 fruit-fly or nematodes (Fig 1 A). We estimated that the overall identity in aminoacidic sequence
319 between zebrafish and human PERK is around 58% (Figure 1 A). Regarding the catalytic site
320 of PERK, which is vital for GSK binding (2012.Axten.JMedChem), the identity between
321 human and zebrafish is around 51% (Figure 1 A). We focused the analysis to compare
322 specifically the 12 vital amino acids for GSK binding to PERK's catalytic site

323 (2012.Axten.JMedChem, 2020.Chintha.RSCAdvances) and found that only human
324 hydrophobic valine 651 is substituted for another hydrophobic amino acid, the isoleucine 651,
325 in the zebrafish amino acid sequence (Figure 1 B, Valine-651 in yellow; Isoleucine-671 in red).
326 Knowing these similarities in the aminoacidic content between human and zebrafish
327 PERK, we next compared protein tertiary structure . To do so, we visualized the binding of
328 GSK (Figure 1 C - purple) to zebrafish (Figure 1 C – darker blue) and human (Figure 1 C –
329 lighter blue) PERK with ChimeraX software, which showed high similarity in structure. Using
330 the same software, we obtained the root-mean-square deviation (RMSD), a measure of the
331 average distance between the atoms of zebrafish and human PERK, for the active site and total
332 structure of the protein. The results indicate that both structures present a high level of
333 similarity (Figure 1 D). Additionally, we performed a Ramachandran plot analysis in SWISS-
334 MODEL and obtained the Ramachandran outliers for the total protein of zebrafish PERK,
335 which indicated that around 90% of the angles established between atoms in the zebrafish
336 protein are similar with the ones in human zebrafish (Figure 1 D).
337 The majority of the amino acid residues that are vital for GSK binding to human PERK
338 are similar zebrafish PERK, suggesting a high probability of binding between GSK and the
339 zebrafish PERK, which prompted us to evaluate the bioactivity of GSK in zebrafish larvae.
340
341 **3.2 PERK is essential for zebrafish embryonic survival**
342
343 Following the bioinformatic analysis suggesting that GSK should efficiently bind to zebrafish
344 PERK, we incubated this PERK inhibitor in zebrafish larvae to assess the survival and hatching
345 rate and to investigate the mechanism of action of GSK (Figure 2 A).
346 First, we evaluated the survival and hatching rate of fish treated with different
347 concentrations of GSK over time. Regarding survival, there is a concentration-dependent

348 decrease in survival at 76 hpf (Figure 2 B). At such timepoint, the survival rate of zebrafish
349 larvae treated with 10 μM GSK significantly decreased to 50% (Figure 2 B). We also calculated
350 the LC_{50} for GSK at 76 hpf, which was 8.8 ± 0.2 μM. We selected 10 μM GSK for following
351 experiments since it produced a significant effect on zebrafish survival. Results indicate that in
352 surviving zebrafish, the hatching rate remains unchanged after treatment with concentrations
353 of GSK up to 10 μM (Figure 2 C).

354 Next, we tested the mechanism of action of GSK in the zebrafish larvae at 76 hpf by
355 monitoring the activation of the ISR pathway via western blot (Figure 2 D *i*). Results show that
356 treatment with GSK (10 μM, 72h) decreases the phosphorylation of eIF2α and the levels of
357 ATF4 and CHOP (Figure 2 D *ii-vi*), which indicates that the GSK is bioactive and is inhibiting
358 PERK pathway.

359 The results suggest that the chosen PERK inhibitor (GSK, 10 μM) produces toxic
360 effects on larvae survival and effectively inhibits the PERK pathway in zebrafish .

361

362 **3.3 PERK is essential for zebrafish skeletal development**

363

364 One of the hallmarks of WRS is the presence of skeletal dysplasia (2010.Julier.OrphJRareDis).
365 Considering that GSK effectively inhibits PERK in zebrafish, we tested if its incubation would
366 induce changes in the skeletal development of zebrafish, mimicking the phenotype that occurs
367 in WRS patients.

368 The daily monitoring of fish development showed that, within the surviving fish treated
369 with 10 μM of GSK, there is a significant increase in the percentage of larvae with
370 morphological defects when compared to control (Figure 3 A *i*). The data also suggest that the
371 percentage of defective larvae increases with duration of treatment (Figure 3 A *i*). We observed
372 that, at 76 hpf, the majority of the defective larvae treated with 10 μM of GSK presented

373 lordosis and the remaining few presented scoliosis (Figures 3 A *ii* - *iv*). Treatment with GSK
374 (10 μM, 76 hpf) causes a 20 ± 4.6 degree curvature of zebrafish tail (Figure 3 B). Skeletal
375 changes at 76 hpf are accompanied by a significant decrease in larval body size (Figure 3 C).
376 To ascertain if skeletal defects or abnormal muscle contraction induced the morphological
377 defects seen in GSK-treated larvae, we used d-tubocurarine (dTC), a muscle relaxant that acts
378 as an antagonist of the nicotinic receptors blocking muscle contraction
379 (2002.Buss.JNeurophysiol) and decreasing TEER in zebrafish (2020.Guzman.EnvironSciEur).
380 Results suggest that dTC significantly decreased larvae TEER to the head (Figure 3 D *i*) and
381 the tail (Figure 3 D *ii*), in concentrations higher than 0.3 mM. d-tubocurarine 3mM treatment
382 failed to recover morphological defects in GSK-treated larva defects (Figure 3 E), which
383 indicates that these defects are more likely due to alterations in skeletal development than to
384 increased muscle contraction.

385 These results suggest that PERK is essential for zebrafish skeletal development and its
386 inhibition induces skeletal abnormalities in zebrafish larvae, mimicking WRS hallmarks in
387 humans.

388

389 **3.4 PERK inhibition delays endocrine pancreas development and limits glucose uptake**
390 **in zebrafish**

391

392 The second hallmark of WRS in humans is neonatal diabetes, which results from decreased β-
393 cell mass and impaired insulin production (2020.Sumegi.BMCPediatrics, 2009.Rubio-
394 Cabezas.JCEM). Therefore, we explored if inhibiting PERK in zebrafish would decrease the
395 mass of insulin-producing β-cells without altering the mass of other cells from the endocrine
396 (somatostatin-producing δ-cells) and exocrine (elastase producing cells) pancreas.

397 To understand how PERK inhibition affects pancreas development, we used two double
398 transgenic fish: 1) Tg(*ins:GFP, sst:mCherry*) that express GFP in insulin-producing β-cells
399 and mCherry in somatostatin-producing δ-cells from the endocrine pancreas; and 2)
400 Tg(*ins:GFP, ela:mCherry*) that express GFP in insulin-producing β-cells and mCherry in
401 elastase-producing exocrine pancreas (Figure 4 A); and estimated the labelled area as a measure
402 for cell mass. We inhibited PERK in these transgenics using GSK in two treatment approaches:
403 one where exposure started at 4 hpf (Figure 4 B *iv)*, before the endocrine pancreas is formed,
404 and a second where exposure started at 76 hpf (Figure 4 B *i)*, when the principal islet is already
405 formed (2009.Tiso.MolCelEndocrinol).

406 GSK (10 μM) significantly decreases the area of *ins:GFP* and *sst:mCherry* labelling at
407 28 hpf (Figure 4 C *i,* D *i*). However, this transient decrease is overcome in the following
408 timepoints, where the labelled areas are similar between treatments (Figure 4 C *i,* D *i*).
409 Regarding elastase, *ela:mCherry* was only detected at 148 hpf, and no differences were found
410 between treated and non-treated larvae (Figure 4 E *i*). These results suggest that inhibiting
411 PERK from the early developmental time points delays the development of endocrine pancreas,
412 without permanently affecting the mass of either endocrine or exocrine pancreatic structures.
413 Finally, GSK exposure after the principal islet is formed (at 76 hpf) did not alter the area of
414 any of the labels (Figure 4 C *ii,* D *ii*, E *ii*), which suggests that role of PERK in pancreatic
415 development in zebrafish is vital in early embryonic stages.

416 Since inhibiting PERK delayed pancreatic development, we tested if this affected
417 glucose homeostasis in zebrafish. To do so, we evaluated the incorporation of a fluorescent
418 glucose probe (2-NBDglucose), in zebrafish treated with GSK (10 μM) from 4 to 76 hpf (Figure
419 5 A). Previous studies showed that diabetes zebrafish models present decreased uptake of 2-
420 NBDglucose (2013.Lee.ACSChemBiol). The incorporation of 2-NBDglucose was analysed in
421 neuromasts, whose location and high surface area enable efficient probe diffusion. PERK

422 inhibition decreased the number of 2-NBDglucose labelled neuromasts in comparison with
423 control (Figure 5 A, B). Neuromast labelling with Mitotracker Deep Red (1 μM), which is
424 independent from glucose uptake, shows that GSK treatment does not affect neuromast
425 formation. These results suggest that PERK inhibition decreased 2-NBDglucose signal by
426 decreasing glucose uptake.

427 Overall, PERK inhibition delayed pancreatic development and induced a diabetic-like
428 phenotype, which is characteristic of WRS.

429

430 **3.5 PERK inhibition impairs zebrafish neuromuscular function**

431

432 WRS includes broad-spectrum manifestations such as difficulty in movement, early
433 neurodegeneration and motor neuropathy in addition to skeletal dysplasia and neonatal diabetes
434 (2010.Julier.OrphJRarDis). We hypothesized that inhibiting PERK in zebrafish larvae
435 produces similar neuromuscular alterations. To test this hypothesis, we evaluated the effect of
436 PERK inhibition on spontaneous movements of zebrafish embryos at 28 hpf and the TEER on
437 larvae in response to touch on the head and tail at 76hpf (2019.Zindler.EcotoxEnvironSafety;
438 2019.Roberts.PlosOne; 2023.Wyl.Chemosphere)

439 Results show that GSK (10 μM) increases spontaneous movements in comparison to
440 control larvae (Figure 6 A *ii*). Regarding the TEER at 76hpf, GSK (10 μM) significantly
441 decreases the responses to head and tail touches (Figure 6 B *i* and *ii*). These results indicate
442 that GSK impairs neuromuscular function in zebrafish larva, mimicking WRS phenotypes.

443 One of the other components that can influence neuromuscular function is the integrity
444 of the musculature (2008.Menelaou.EurJNeurosci). Thus, we assessed said integrity through a
445 muscle birefringence assay. Birefringence results from diffraction of polarized light through
446 the pseudocrystalline arrangement of fish muscle sarcomeres (Figure 6 C *i*)

447 (2012.Berger.BBRC). Thus, zebrafish musculature is seen under polarized light as a white
448 structure on a black background (Figure 6 C *ii*). In fish treated with 10 µM GSK, birefringence
449 intensity decreased around 40%, which reflects an impairment in the muscular integrity of fish
450 treated with PERK's inhibitor (Figure 6 C *iii*).

451 Thus, PERK inhibition mimics the difficulty in movement existing in WRS patients.
452 Additionally, we suggest that these difficulties may be caused by GSK-driven impairment in
453 neuromuscular function and muscle integrity.

454

455 **3.6 PERK inhibition impairs zebrafish cardiac function**

456

457 Broad-spectrum manifestations of WRS include cardiac defects, with some patients suffering
458 from congenital cardiac malformations such as enlargement of the heart chambers and changes
459 in cardiac rhythm (2004.Senée.Diabetes; 1997.Thorton.PediatrPatholLabMed). We evaluated
460 if zebrafish larvae treated with the PERK inhibitor GSK demonstrated functional and
461 morphological abnormalities at the cardiac level.

462 We found that larvae treated with 10 µM of the PERK inhibitor develop cardiac oedema
463 (Figure 7 A *i*) as early as 28 hpf, extending to 76 hpf (Figure 7 A *ii, iii*). To ascertain if the
464 cardiac oedema was associated with defective cardiac function, we evaluated the heart rate and
465 atrio-ventricular coordination of larvae at 76 hpf. 10 µM GSK decreased the heart rate in
466 zebrafish larva from 160 beats per minute (bpm) in control larvae to 110 bpm in treated larvae
467 (Figure 7 B *i*). A more detailed analysis of the larvae's heart showed that despite presenting
468 bradycardia, larvae treated with 10 µM GSK preserve atrio-ventricular coordination (Figure 7
469 B *ii*).

470 The inhibition of PERK during the embryonic development of zebrafish induced
471 cardiac oedema and elicited bradycardia while preserving atrio-ventricular coordination.

472 **4. Discussion**

473

474 The cause of WRS has long been identified as loss-of-function mutations in the gene encoding
475 PERK (2010.Julier.OrphJRareDis), however, there are still no effective treatments for WRS
476 nor *in vivo* models available for large-scale testing of potential therapies. Here, we developed
477 a pharmacological zebrafish model of WRS suitable for large-scale therapeutic testing. Our
478 WRS model mimics the hallmarks of WRS such as skeletal defects and neonatal diabetes, as
479 well as the more broad-spectrum manifestations such as cardiac and neuromuscular alterations.

480 Regarding the skeleton and pancreas, zebrafish and humans share great similarities in
481 anatomy and physiology. Skeletal development of zebrafish and humans is highly similar since
482 all relevant skeletal cell types and development pathways are conserved between the two
483 species (2019.Bergen.FrontEndcrinol). WRS patients present short stature and skeletal
484 dysplasia, particularly noticeable in long bones, pelvis and vertebrae
485 (2010.Julier.OrphJRareDis). The proposed mechanism for skeletal impairments in WRS is that
486 PERK's loss-of-function delays the differentiation and proliferation of osteoblasts and
487 decreases the secretion of type I collagen. As these are essential factors for normal bone
488 development, PERK's loss-of-function decreases bone mineralization
489 (2008.Wei.JCellPhysiol). Mice with PERK ablation exhibit postnatal growth retardation, bone
490 loss and skeletal dysplasia (2001.Zhang.CellGrowthDev, 2003.Li.Endocrinol,
491 2020.Guo.CellDeathDis). We show that GSK treatment also decreased body length and
492 induced skeletal defects, therefore indicating that zebrafish can mimic human skeletal
493 impairments and be used to model bone diseases.

494 Little is known about the origin of the diabetes in WRS patients besides that it is not
495 autoimmune since they do not present antibodies specific for type I diabetes
496 (2010.Julier.OrphJRareDis). Instead, WRS patients present a hypoplastic pancreas, with

497 smaller insulin-secreting β cells within the Langerhans islets (2020.Welters.OrpJRareDis).
498 Accordingly, PERK ablation in mice reduced the mass of insulin-producing β cells and induced
499 hyperglycaemia. These phenotypes originate due to decreased proliferation and defective
500 proinsulin maturation (2009.Feng.BMCMolCellBiol, 2001.Harding.MolCell,
501 2006.Zhang.CellMetab) rather than peripheral resistance to the action of insulin
502 (2001.Harding.MolCell) or increased cell death (2006.Zhang.CellMetab,
503 2008.Wei.JCellPhysiol). Our results suggest that inhibiting PERK in zebrafish delayed the
504 development of endocrine pancreas, which aligns with WRS in humans and mice. However,
505 this delay in zebrafish is only present in the early developmental days, without altering the final
506 morphology of the pancreas once the developmental stage is complete. One hypothesis to
507 explain this time-dependent recovery in β-cell mass in larvae treated with GSK is the elevated
508 capacity of zebrafish to regenerate pancreatic tissue (2009.Moss.Diabetes,
509 2007.Pisharath.MechDev). In contrast with zebrafish, human and mice pancreas have little
510 regenerative capacity, which can explain why in both cases, the loss of β-cell mass upon PERK
511 inhibition extends until older stages (2009.Moss.Diabetes). The role of PERK in zebrafish
512 tissue regeneration remains unexplored and we suggest that PERK-independent mechanisms
513 allow pancreatic recovery upon decreased β-cell mass. Furthermore, only when PERK was
514 inhibited before the formation of the principal islet of Langerhans was it possible to see the
515 delay in pancreatic development, which is in accordance with previous findings showing that
516 genetically ablating PERK in adult mice did not alter β cell mass or glycemia
517 (2006.Zhang.CellMetab).

518 Regarding the exocrine pancreas, the earliest timepoint allowing detection of the elastase
519 reporter was 148 hpf. At that time point, we found no effect of GSK2606414 in the mass of
520 elastase-producing cells. While different mechanisms regulate development of the exocrine
521 and endocrine pancreas, we cannot rule out that our zebrafish model may present differences

522 in the mass of elastase-producing cells in earlier timepoints, as happens with β-cells. Previous
523 clinical studies showed that only 25% of WRS patients present exocrine pancreas insufficiency,
524 which makes it a broad-spectrum phenotype of WRS (2010.Julier.OrphJRareDis,
525 2010.Ozbek.PedDiabetes). In mice, PERK KO induces exocrine pancreas cell death by oncosis
526 (2015_Balvan_PlosOne; 2007.Iida.BMCCellBiol), which suggests that an extended exposure
527 to GSK might induce damage to the exocrine pancreas.

528 Regarding the mechanism of insulin production in β-cells, insulin is folded and matured
529 in the endoplasmic reticulum, which basally activates PERK. Studies show that deleting PERK
530 in rodents decreases β-cells mass, which reduces cell-cell contacts that are important for
531 increasing glucose-stimulated insulin secretion therefore provoking hyperglycemia
532 (2006.Zhang.CellMetab). Our results also suggest that although β-cell mass recovers insulin
533 production might remain compromised. In PERK-inhibitied zebrafish, glucose uptake is
534 decreased, which allows us to hypothesize that PERK inhibition may decrease insulin
535 production and induce hyperglycemia in zebrafish, which is in line with what occurs in WRS
536 rodent models (2006.Zhang.CellMetab).

537 Although skeletal dysplasia and early onset diabetes are essential clinical manifestations
538 for the diagnosis of WRS, the variety of disease-causing mutations in the PERK gene elicits a
539 broad-spectrum of WRS symptoms, such as cardiac and neuromuscular changes (2019.Asl.
540 JPediatEndocrinMetab, 2004.Senée.Diabetes; 1997.Thorton.PediatrPatholLabMed). Zebrafish
541 treated with GSK also developed cardiac and neuromuscular changes, as evidenced by the
542 increased cardiac oedema, higher spontaneous movement, decreased heart rate and lower
543 TEER. Regarding cardiac alterations, clinicians reported multiple cases of WRS patients with
544 cardiac malformations such as double outlet right ventricle and atrio-ventricular dilatation
545 (1997.Thorton.PediatrPatholLabMed; 2018.Bejiqi.MedArch). Mice with PERK conditional
546 knock out show alterations in the formation of heart valves (2020.Shimizu.SciRep). Zebrafish

547 present advantages in relation to other mammals when it comes to studying the cardiovascular
548 system, namely: 1) being able to observe the formation of the heart chambers, cardiac
549 contraction, bloodflow, and vessels *in vivo* by non-invasive techniques and 2) not being fully
550 dependent upon a functional cardiovascular system in the early development stages since they
551 get sufficient oxygen by passive diffusion, which allows the detection of cardiovascular
552 malformations that in mammals would be lethal (2016.Bournele.HeartFailRev). Our data
553 shows that PERK inhibition in zebrafish induces morphologic and functional cardiac
554 alterations, which indicates that this model is suitable to study cardiac alterations in WRS and
555 implicates PERK in cardiac development, although the mechanism is not yet fully understood
556 (2020.Shimizu.SciRep).

557 Regarding neuromuscular function, WRS patients suffer from brain structural
558 abnormalities, microcephaly and muscle weakness (2015.Bruch.JNeuropatholExpNeurol,
559 2010.Julier.OrphJRareDis) however, the mechanisms behind such symptoms are unknown. We
560 assessed the function of neuromuscular systems in the zebrafish larvae treated with GSK by
561 evaluating the spontaneous movement at 28 hpf and the TEER at 76 hpf. Surprisingly, PERK
562 inhibition significantly increased spontaneous tail movements of zebrafish embryos while
563 decreasing the response to touch. One explanation for this apparent paradox might reside in the
564 neuro-muscular circuits that govern both movements. Early spontaneous tail movements in
565 zebrafish arise in a spinal central pattern generator that provides rhythmic depolarizations
566 followed by unilateral muscle contractions to produce the tail coilings. These depolarizations
567 involve interneurons, motor neurons and muscles and are governed by gap junction-mediated
568 neurotransmission (2023.Wyl.Chemosphere; 2019.Zindler.EcotoxEnvironSafety).
569 Contrastingly, the reflex response to touch arises in Rohon-Beard sensory neurons, hindbrain
570 reticulospinal neurons, spinal cord interneurons and secondary motor neurons and are governed
571 by chemical synaptic inputs (2023.Wyl.Chemosphere; 2019.Roberts.PlosOne). Another

572 explanation for decreased reflex response may reside in the presence of skeletal defects. In
573 zebrafish larva treated with GSK, we did not detect a significant appearance of skeletal defects
574 at 28 hpf, the same timepoint of the spontaneous tail coilings, but at 76 hpf, the timepoint of
575 reflex evaluation, there is a significant increase in the number of larvae with skeletal defects
576 that might hinder movement. Nonetheless, the decreased tail coilings in zebrafish larvae upon
577 PERK inhibition suggest that this protein is important for neuronal and muscular development
578 and function.

579 Since GSK-treated zebrafish presented neuromuscular dysfunction, we assessed if GSK
580 had any direct impact in muscle integrity through the birefringence assay. In the case of
581 zebrafish treated with a PERK inhibitor, there is a significant decrease in the intensity of
582 birefringent light, which suggests that there is a decrease in the muscle integrity of the fish.
583 These results are in accordance with recently published data showing that PERK ablation in
584 mice decreases skeletal muscle mass, strength, and force production (2019.Gadot.FASEBJ).
585 Thus, we hypothesize that PERK alters neuromuscular communication by a combination of
586 alterations at the neuronal level with impairments in muscle development.

587

588 **5. Conclusions**

589

590 In this study, we investigated if zebrafish could be used to model WRS by inhibiting PERK.
591 The pharmacological inhibition of PERK mimicked cardinal features of WRS such as skeletal
592 defects and alterations in glucose homeostasis. Inhibiting PERK in zebrafish larvae also
593 produced the broad-spectrum manifestations of human WRS such as cardiac alterations and
594 neuromuscular deficits. These results validate the use of zebrafish to produce an *in vivo* WRS
595 model for large scale testing, aiming to find safer, effective, and less invasive therapeutic
596 options for WRS patients.

597

Declarations

Funding

Work in JMAO's lab was supported by the FCT – Fundação para a Ciência e a Tecnologia, Portugal – (UIDB/04378/2020; UIDP/04378/2020; LA/P/0140/2020). LMA acknowledges FCT for PhD fellowship (SFRH/BD/138451/2018). BRP acknowledges FCT for funding through program DL57/2016 - Norma transitória (DL57/2016/CP1346/CT0016). JB's laboratory was supported by Fundação para a Ciência e a Tecnologia (FCT) in the framework of the project PTDC/BIA-MOL/3834/2021. JB was supported by a FCT contract (CEECIND/03482/2018).

Competing Interests

The authors have no relevant financial or non-financial interests to disclose.

614 **References**

615 ALMEIDA, L. M., PINHO, B. R., DUCHEN, M. R. & OLIVEIRA, J. M. A. (2022). The
616 PERKs of mitochondria protection during stress: insights for PERK modulation in
617 neurodegenerative and metabolic diseases. Biol Rev Camb Philos Soc.

618 ASL, S. N., VAKILI, R., VAKILI, S., SOHEILIPOUR, F., HASHEMIPOUR, M.,
619 GHAHRAMANI, S., DE FRANCO, E. & YAGHOOTKAR, H. (2019). Wolcott-Rallison
620 syndrome in Iran: a common cause of neonatal diabetes. J Pediatr Endocrinol Metab 32(6),
621 607-613.

622 AXTEN, J. M., MEDINA, J. R., FENG, Y., SHU, A., ROMERIL, S. P., GRANT, S. W., LI,
623 W. H., HEERDING, D. A., MINTHORN, E., MENCKEN, T., ATKINS, C., LIU, Q.,
624 RABINDRAN, S., KUMAR, R., HONG, X., GOETZ, A., STANLEY, T., TAYLOR, J. D.,
625 SIGETHY, S. D., TOMBERLIN, G. H., HASSELL, A. M., KAHLER, K. M., SHEWCHUK,
626 L. M. & GAMPE, R. T. (2012). Discovery of 7-methyl-5-(1-{[3-
627 (trifluoromethyl)phenyl]acetyl}-2,3-dihydro-1H-indol-5-yl)-7H-p yrrolo[2,3-d]pyrimidin-4-
628 amine (GSK2606414), a potent and selective first-in-class inhibitor of protein kinase R (PKR)-
629 like endoplasmic reticulum kinase (PERK). J Med Chem 55(16), 7193-207.

630 BEJIQI, R., RETKOCERI, R., ZEKA, N., BEJIQI, R. & BEJIC, S. (2018). An Infant With
631 Neonatal Diabetes and Double Outlet Right Ventricle - Wolcott- Rallison syndrome. Med Arch
632 72(4), 289-291.

633 BERGER, J., SZTAL, T. & CURRIE, P. D. (2012). Quantification of birefringence readily
634 measures the level of muscle damage in zebrafish. Biochem Biophys Res Commun 423(4),
635 785-8.

636 BERGEN, D. J. M., KAGUE, E. & HAMMOND, C. L. (2019). Zebrafish as an Emerging
637 Model for Osteoporosis: A Primary Testing Platform for Screening New Osteo-Active
638 Compounds. Front Endocrinol (Lausanne) 10, 6.

639 BOURNELE, D. & BEIS, D. (2016). Zebrafish models of cardiovascular disease. Heart Fail
640 Rev 21(6), 803-813.
641 BRUCH, J., KURZ, C., VASILJEVIC, A., NICOLINO, M., ARZBERGER, T. &
642 HOGLINGER, G. U. (2015). Early Neurodegeneration in the Brain of a Child Without
643 Functional PKR-like Endoplasmic Reticulum Kinase. J Neuropathol Exp Neurol 74(8), 850-7.
644 BUSS, R. R. & DRAPEAU, P. (2002). Activation of embryonic red and white muscle fibers
645 during fictive swimming in the developing zebrafish. J Neurophysiol 87(3), 1244-51.
646 CHINTHA, C., CARLESSO, A., GORMAN, A. M., SAMALI, A. & ERIKSSON, L. A.
647 (2019). Molecular modeling provides a structural basis for PERK inhibitor selectivity towards
648 RIPK1. RSC Adv 10(1), 367-375.
649 CHOI, T. Y., CHOI, T. I., LEE, Y. R., CHOE, S. K. & KIM, C. H. (2021). Zebrafish as an
650 animal model for biomedical research. Exp Mol Med 53(3), 310-317.
651 DELEPINE, M., NICOLINO, M., BARRETT, T., GOLAMAULLY, M., LATHROP, G. M.
652 & JULIER, C. (2000). EIF2AK3, encoding translation initiation factor 2-alpha kinase 3, is
653 mutated in patients with Wolcott-Rallison syndrome. Nat Genet 25(4), 406-9.
654 EUFRASIO, A., PERROD, C., FERREIRA, F. J., DUQUE, M., GALHARDO, M. & BESSA,
655 J. (2020). In Vivo Reporter Assays Uncover Changes in Enhancer Activity Caused by Type 2
656 Diabetes-Associated Single Nucleotide Polymorphisms. Diabetes 69(12), 2794-2805.
657 FENG, D., WEI, J., GUPTA, S., MCGRATH, B. C. & CAVENER, D. R. (2009). Acute
658 ablation of PERK results in ER dysfunctions followed by reduced insulin secretion and cell
659 proliferation. BMC Cell Biol 10, 61.
660 GALLOT, Y. S., BOHNERT, K. R., STRAUGHN, A. R., XIONG, G., HINDI, S. M. &
661 KUMAR, A. (2019). PERK regulates skeletal muscle mass and contractile function in adult
662 mice. FASEB J 33(2), 1946-1962.

663 GUO, X., AVILES, G., LIU, Y., TIAN, R., UNGER, B. A., LIN, Y. T., WIITA, A. P., XU, K.,
664 CORREIA, M. A. & KAMPMANN, M. (2020). Mitochondrial stress is relayed to the cytosol
665 by an OMA1-DELE1-HRI pathway. Nature 579(7799), 427-432.
666 GUZMAN, L., BESA, G., LINARES, D., GONZÁLEZ, L., PONT, C., BARTOLINI, M.,
667 HAIGIS, A.C., LEGRADI, J., MUÑOZ-TORRERO, D., GÓMEZ-CATALÁN, J., &
668 BARENYS. M. (2020) Evaluation of the effects of acetylcholinesterase inhibitors in the
669 zebrafish touch-evoked response: quantitative vs. qualitative assessment. Environ Sci Eur 32,
670 145.
671 HARDING, H. P., ZENG, H., ZHANG, Y., JUNGRIES, R., CHUNG, P., PLESKEN, H.,
672 SABATINI, D. D. & RON, D. (2001). Diabetes mellitus and exocrine pancreatic dysfunction
673 in perk-/- mice reveals a role for translational control in secretory cell survival. Mol Cell 7(6),
674 1153-63.
675 HOYBERGHS, J., BARS, C., AYUSO, M., VAN GINNEKEN, C., FOUBERT, K. & VAN
676 CRUCHTEN, S. (2021). DMSO Concentrations up to 1% are Safe to be Used in the Zebrafish
677 Embryo Developmental Toxicity Assay. Front Toxicol 3, 804033.
678 IIDA, K., LI, Y., MCGRATH, B. C., FRANK, A. & CAVENER, D. R. (2007). PERK eIF2
679 alpha kinase is required to regulate the viability of the exocrine pancreas in mice. BMC Cell
680 Biol 8, 38.
681 JUMPER, J., EVANS, R., PRITZEL, A., GREEN, T., FIGURNOV, M., RONNEBERGER,
682 O., TUNYASUVUNAKOOL, K., BATES, R., ŽÍDEK, A., POTAPENKO, A., BRIDGLAND,
683 A., MEYER, C., KOHL, S. A. A., BALLARD, A. J., COWIE, A., ROMERA-PAREDES, B.,
684 NIKOLOV, S., JAIN, R., ADLER, J., BACK, T., PETERSEN, S., REIMAN, D., CLANCY,
685 E., ZIELINSKI, M., STEINEGGER, M., PACHOLSKA, M., BERGHAMMER, T.,
686 BODENSTEIN, S., SILVER, D., VINYALS, O., SENIOR, A. W., KAVUKCUOGLU, K.,

687 KOHLI, P., HASSABIS, D. (2021). Highly accurate protein structure prediction with
688 AlphaFold. Nature 596(7873): 583-589.
689 JULIER, C. & NICOLINO, M. (2010). Wolcott-Rallison syndrome. Orphanet J Rare Dis 5, 29.
690 KAWAKAMI, K., SHIMA, A. & KAWAKAMI, N. (2000). Identification of a functional
691 transposase of the Tol2 element, an Ac-like element from the Japanese medaka fish, and its
692 transposition in the zebrafish germ lineage. Proc Natl Acad Sci U S A 97(21), 11403-8.
693 KIMMEL, C. B., BALLARD, W. W., KIMMEL, S. R., ULLMANN, B. & SCHILLING, T. F.
694 (1995). Stages of embryonic development of the zebrafish. Dev Dyn 203(3), 253-310.
695 LEE, J., JUNG, D. W., KIM, W. H., UM, J. I., YIM, S. H., OH, W. K. & WILLIAMS, D. R.
696 (2013). Development of a highly visual, simple, and rapid test for the discovery of novel insulin
697 mimetics in living vertebrates. ACS Chem Biol 8(8), 1803-14.
698 LI, Y., IIDA, K., O'NEIL, J., ZHANG, P., LI, S., FRANK, A., GABAI, A., ZAMBITO, F.,
699 LIANG, S. H., ROSEN, C. J. & CAVENER, D. R. (2003). PERK eIF2alpha kinase regulates
700 neonatal growth by controlling the expression of circulating insulin-like growth factor-I
701 derived from the liver. Endocrinology 144(8), 3505-13.
702 MARTINEZ, R., NAVARRO-MARTIN, L., LUCCARELLI, C., CODINA, A. E., RALDUA,
703 D., BARATA, C., TAULER, R. & PINA, B. (2019). Unravelling the mechanisms of PFOS
704 toxicity by combining morphological and transcriptomic analyses in zebrafish embryos. Sci
705 Total Environ 674, 462-471.
706 MENELAOU, E., HUSBANDS, E. E., POLLET, R. G., COUTTS, C. A., ALI, D. W. &
707 SVOBODA, K. R. (2008). Embryonic motor activity and implications for regulating
708 motoneuron axonal pathfinding in zebrafish. Eur J Neurosci 28(6), 1080-96.
709 MOSS, J. B., KOUSTUBHAN, P., GREENMAN, M., PARSONS, M. J., WALTER, I. &
710 MOSS, L. G. (2009). Regeneration of the pancreas in adult zebrafish. Diabetes 58(8), 1844-
711 51.

712 MORENO, J. A., HALLIDAY, M., MOLLOY, C., RADFORD, H., VERITY, N., AXTEN, J.
713 M., ORTORI, C. A., WILLIS, A. E., FISCHER, P. M., BARRETT, D. A. & MALLUCCI, G.
714 R. (2013). Oral treatment targeting the unfolded protein response prevents neurodegeneration
715 and clinical disease in prion-infected mice. Sci Transl Med 5(206), 206ra138.
716 OLIVEIRA, N. A. S., PINHO, B. R., PINTO, J., GUEDES DE PINHO, P. & OLIVEIRA, J.
717 M. A. (2024). Edaravone counteracts redox and metabolic disruptions in an emerging zebrafish
718 model of sporadic ALS. Free Radic Biol Med 217, 126-140.
719 OZBEK, M. N., SENEE, V., AYDEMIR, S., KOTAN, L. D., MUNGAN, N. O., YUKSEL,
720 B., JULIER, C. & TOPALOGLU, A. K. (2010). Wolcott-Rallison syndrome due to the same
721 mutation (W522X) in EIF2AK3 in two unrelated families and review of the literature. Pediatr
722 Diabetes 11(4), 279-85.
723 PETTERSEN, E. F., GODDARD, T. D., HUANG, C. C., MENG, E. C., COUCH, G. S.,
724 CROLL, T. I., MORRIS, J. H., FERRIN, T. E. (2021). UCSF ChimeraX: Structure
725 visualization for researchers, educators, and developers. Protein Sci 30(1): 70-82.
726 PINHO, B. R., REIS, S. D., GUEDES-DIAS, P., LEITAO-ROCHA, A., QUINTAS, C.,
727 VALENTAO, P., ANDRADE, P. B., SANTOS, M. M. & OLIVEIRA, J. M. (2016).
728 Pharmacological modulation of HDAC1 and HDAC6 in vivo in a zebrafish model: Therapeutic
729 implications for Parkinson's disease. Pharmacol Res 103, 328-39.
730 PINHO, B. R., REIS, S. D., HARTLEY, R. C., MURPHY, M. P. & OLIVEIRA, J. M. A.
731 (2019). Mitochondrial superoxide generation induces a parkinsonian phenotype in zebrafish
732 and huntingtin aggregation in human cells. Free Radic Biol Med 130, 318-327.
733 PINHO, B. R., SANTOS, M. M., FONSECA-SILVA, A., VALENTAO, P., ANDRADE, P. B.
734 & OLIVEIRA, J. M. (2013). How mitochondrial dysfunction affects zebrafish development
735 and cardiovascular function: an in vivo model for testing mitochondria-targeted drugs. Br J
736 Pharmacol 169(5), 1072-90.

PISHARATH, H., RHEE, J. M., SWANSON, M. A., LEACH, S. D. & PARSONS, M. J. (2007). Targeted ablation of beta cells in the embryonic zebrafish pancreas using E. coli nitroreductase. Mech Dev 124(3), 218-29.

PRINCE, V. E., ANDERSON, R. M. & DALGIN, G. (2017). Zebrafish Pancreas Development and Regeneration: Fishing for Diabetes Therapies. Curr Top Dev Biol 124, 235-276.

ROBERTS, A. C., CHORNAK, J., ALZAGATITI, J. B., LY, D. T., BILL, B. R., TRINKELLER, J., PEARCE, K. C., CHOE, R. C., CAMPBELL, C. S., WONG, D., DEUTSCH, E., HERNANDEZ, S. & GLANZMAN, D. L. (2019). Rapid habituation of a touch-induced escape response in Zebrafish (Danio rerio) Larvae. PLoS One 14(4), e0214374.

RUBIO-CABEZAS, O., PATCH, A. M., MINTON, J. A., FLANAGAN, S. E., EDGHILL, E. L., HUSSAIN, K., BALAFREJ, A., DEEB, A., BUCHANAN, C. R., JEFFERSON, I. G., MUTAIR, A., NEONATAL DIABETES INTERNATIONAL COLLABORATIVE, G., HATTERSLEY, A. T. & ELLARD, S. (2009). Wolcott-Rallison syndrome is the most common genetic cause of permanent neonatal diabetes in consanguineous families. J Clin Endocrinol Metab 94(11), 4162-70.

SENEE, V., VATTEM, K. M., DELEPINE, M., RAINBOW, L. A., HATON, C., LECOQ, A., SHAW, N. J., ROBERT, J. J., ROOMAN, R., DIATLOFF-ZITO, C., MICHAUD, J. L., BIN-ABBAS, B., TAHA, D., ZABEL, B., FRANCESCHINI, P., TOPALOGLU, A. K., LATHROP, G. M., BARRETT, T. G., NICOLINO, M., WEK, R. C. & JULIER, C. (2004). Wolcott-Rallison Syndrome: clinical, genetic, and functional study of EIF2AK3 mutations and suggestion of genetic heterogeneity. Diabetes 53(7), 1876-83.

SHIMIZU, T., MARUYAMA, K., KAWAMURA, T., URADE, Y. & WADA, Y. (2020). PERK participates in cardiac valve development via fatty acid oxidation and endocardial-mesenchymal transformation. Sci Rep 10(1), 20094.

761 SILVA, R. F. O., PINHO, B. R., SANTOS, M. M. & OLIVEIRA, J. M. A. (2022). Disruptions
762 of circadian rhythms, sleep, and stress responses in zebrafish: New infrared-based activity
763 monitoring assays for toxicity assessment. Chemosphere 305, 135449.
764 SMITH, L. L., BEGGS, A. H. & GUPTA, V. A. (2013). Analysis of skeletal muscle defects in
765 larval zebrafish by birefringence and touch-evoke escape response assays. J Vis Exp (82),
766 e50925.
767 SUMEGI, A., HENDRIK, Z., GALL, T., FELSZEGHY, E., SZAKSZON, K., ANTAL-
768 SZALMAS, P., BEKE, L., PAPP, A., MEHES, G., BALLA, J. & BALLA, G. (2020). A novel
769 splice site indel alteration in the EIF2AK3 gene is responsible for the first cases of Wolcott-
770 Rallison syndrome in Hungary. BMC Med Genet 21(1), 61.
771 STENGEL, D., ZINDLER, F. & BRAUNBECK, T. (2017). An optimized method to assess
772 ototoxic effects in the lateral line of zebrafish (Danio rerio) embryos. Comp Biochem Physiol
773 C Toxicol Pharmacol 193, 18-29.
774 TEAME, T., ZHANG, Z., RAN, C., ZHANG, H., YANG, Y., DING, Q., XIE, M., GAO, C.,
775 YE, Y., DUAN, M. & ZHOU, Z. (2019). The use of zebrafish (Danio rerio) as biomedical
776 models. Anim Front 9(3), 68-77.
777 THORNTON, C. M., CARSON, D. J. & STEWART, F. J. (1997). Autopsy findings in the
778 Wolcott-Rallison syndrome. Pediatr Pathol Lab Med 17(3), 487-96.
779 TISO, N., MORO, E. & ARGENTON, F. (2009). Zebrafish pancreas development. Mol Cell
780 Endocrinol 312(1-2), 24-30.
781 TRINH, M. A., KAPHZAN, H., WEK, R. C., PIERRE, P., CAVENER, D. R. & KLANN, E.
782 (2012). Brain-specific disruption of the eIF2alpha kinase PERK decreases ATF4 expression
783 and impairs behavioral flexibility. Cell Rep 1(6), 676-88.
784 TZAKIS, A. G., NUNNELLEY, M. J., TEKIN, A., BUCCINI, L. D., GARCIA, J., UCHIDA,
785 K., NEVILLE, H. L., NARES, M. A., RUIZ, P. & BODAMER, O. (2015). Liver, pancreas and

786 kidney transplantation for the treatment of Wolcott-Rallison syndrome. Am J Transplant 15(2),
787 565-7.
788 VARADI, M., ANYANGO, S., DESHPANDE, M., NAIR, S., NATASSIA, C.,
789 YORDANOVA, G., YUAN, D., STROE, O., WOOD, G., LAYDON, A., ŽÍDEK, A., GREEN,
790 T., TUNYASUVUNAKOOL, K., PETERSEN, S., JUMPER, J., CLANCY, E., GREEN, R.,
791 VORA, A., LUTFI, M., FIGURNOV, M., COWIE, A., HOBBS, N., KOHLI, P.,
792 KLEYWEGT, G., BIRNEY, E., HASSABIS, D., VELANKAR, S. (2022). "AlphaFold Protein
793 Structure Database: massively expanding the structural coverage of protein-sequence space
794 with high-accuracy models." Nucleic Acids Res 50(D1): D439-d444.
795 VON WYL, M., KONEMANN, S. & VOM BERG, C. (2023). Different developmental
796 insecticide exposure windows trigger distinct locomotor phenotypes in the early life stages of
797 zebrafish. Chemosphere 317, 137874.
798 WANG, L., KONG, H., JIN, M., LI, X., STOIKA, R., LIN, H. & LIU, K. (2020). Synthesis of
799 disaccharide modified berberine derivatives and their anti-diabetic investigation in zebrafish
800 using a fluorescence-based technology. Org Biomol Chem 18(18), 3563-3574.
801 WATERHOUSE, A., BERTONI, M., BIENERT, S., STUDER, G., TAURIELLO, G.,
802 GUMIENNY, R., HEER, F. T., DE BEER, T. A. P., REMPFER, C., BORDOLI, L., LEPORE,
803 R., SCHWEDE, T. (2018). SWISS-MODEL: homology modelling of protein structures and
804 complexes. Nucleic Acids Res 46(W1): W296-w303.
805 WEI, J., SHENG, X., FENG, D., MCGRATH, B. & CAVENER, D. R. (2008). PERK is
806 essential for neonatal skeletal development to regulate osteoblast proliferation and
807 differentiation. J Cell Physiol 217(3), 693-707.
808 WELTERS, A., MEISSNER, T., KONRAD, K., FREIBERG, C., WARNCKE, K.,
809 JUDMAIER, S., KORDONOURI, O., WURM, M., PAPSCH, M., FITZKE, G., SCHMIDT,

810 S. C., TITTEL, S. R. & HOLL, R. W. (2020). Diabetes management in Wolcott-Rallison
811 syndrome: analysis from the German/Austrian DPV database. Orphanet J Rare Dis 15(1), 100.
812 YONG, J., JOHNSON, J. D., ARVAN, P., HAN, J. & KAUFMAN, R. J. (2021). Therapeutic
813 opportunities for pancreatic beta-cell ER stress in diabetes mellitus. Nat Rev Endocrinol 17(8),
814 455-467.
815 ZHANG, G., WANG, X., GILLETTE, T. G., DENG, Y. & WANG, Z. V. (2019). Unfolded
816 Protein Response as a Therapeutic Target in Cardiovascular Disease. Curr Top Med Chem
817 19(21), 1902-1917.
818 ZHANG, P., MCGRATH, B., LI, S., FRANK, A., ZAMBITO, F., REINERT, J., GANNON,
819 M., MA, K., MCNAUGHTON, K. & CAVENER, D. R. (2002). The PERK eukaryotic
820 initiation factor 2 alpha kinase is required for the development of the skeletal system, postnatal
821 growth, and the function and viability of the pancreas. Mol Cell Biol 22(11), 3864-74.
822 ZHANG, W., FENG, D., LI, Y., IIDA, K., MCGRATH, B. & CAVENER, D. R. (2006). PERK
823 EIF2AK3 control of pancreatic beta cell differentiation and proliferation is required for
824 postnatal glucose homeostasis. Cell Metab 4(6), 491-7.
825 ZINDLER, F., BEEDGEN, F., BRANDT, D., STEINER, M., STENGEL, D., BAUMANN, L.
826 & BRAUNBECK, T. (2019). Analysis of tail coiling activity of zebrafish (Danio rerio)
827 embryos allows for the differentiation of neurotoxicants with different modes of action.
828 Ecotoxicol Environ Saf 186, 109754.
829

830 **Figure legends**

831

832 **Fig. 1** GSK2606414-binding amino acids in PERK are highly similar between zebrafish and
833 human. (**A**) Percentage of identity between human, nematode (*Caenorhabditis elegans*), fruit
834 fly (*Drosophila melanogaster*), zebrafish (*Danio rerio*) and mouse (*Mus musculus*) PERK
835 (total and catalytic domain). (**B**) Detailed analysis of amino acid sequence of the catalytic
836 domain in human and zebrafish PERK that are vital for GSK2606414 binding. The amino acid
837 Valine 651 in human PERK (yellow) is substituted by the Isoleucine 671 (red) in zebrafish
838 PERK. (**C**) Predicted structure for GSK (purple) binding to human (light blue) and zebrafish
839 (dark blue) PERK. PERK with Valine 651 and Isoleucine 671 highlighted in yellow and
840 orange, respectively. (**D**) Root Mean Square Deviation (RMSD) and Ramachandran outliers
841 value for the comparison between human and zebrafish PERK structures and respective
842 reference values.

843

844 **Fig. 2** GSK2606414 concentration dependently inhibits the PERK pathway in zebrafish and
845 limits embryonic survival. (**A**) Protocol and endpoints for the experiments with zebrafish eggs
846 or larvae. (**B**) Survival rate of zebrafish embryos treated with increasing concentrations of
847 GSK2606414 (0.1 – 10 μM) over time (28, 52 and 76 hpf). n = 50-234 larvae, 5 independent
848 breedings, Log-rank (Mantel-Cox) test, $^{*}P < 0.05$ vs. 0 μM GSK. (**C**) Hatching rate of
849 zebrafish embryos treated with increasing concentrations of GSK2606414 (0 – 10 μM) over
850 time (28, 52 and 76 hours post-fertilization (hpf)). n=5 breedings, Two-Way ANOVA: $^{\#}P <$
851 0.05 time effect. (**D**) Western blot with samples from control and 10 μM GSK2606414-treated
852 live zebrafish larvae at 76 hpf: *i*) PERK pathway representation: upon activation, PERK
853 phosphorylates eIF2α, promoting the expression of the transcription factors ATF4 and CHOP.
854 GSK2606414 inhibits PERK kinase activity; *ii*) representative images for labelling of PERK

855 pathway markers - p-eIF2α, eIF2α, ATF4 and CHOP; Quantification of *iii*) eIF2α, *iv*) p-eIF2α,
856 *v*) ATF4 and *vi*) CHOP. $n = 4$ independent experiments, *t*-test: $^{*}P < 0.05$
857
858 **Fig. 3** PERK inhibition induces skeletal abnormalities in zebrafish development. (**A**)
859 Morphological defects in GSK2606414-treated zebrafish larvae. (*i*) Quantification of live larva
860 with morphological defects when treated with increasing concentrations of GSK2606414 at 28,
861 52 and 76 hpf. n= 5 independent experiments. (*ii*) Proportion of skeletal defect types (lordosis
862 or scoliosis) found in live larvae treated with 0 or 10 μM GSK2606414 at 76 hpf. $n = 3$
863 independent experiments. Data in percentage of live larvae at 4 hpf. Two-way ANOVA with
864 significant interaction ($P < 0.05$) between drug concentrations and time; Sidak post-hoc test
865 compared the concentration effect in the percentage of larvae with morphological defects
866 within each time point: $^{*}P < 0.05$; linear trend post-hoc test compared the time effect in the 10
867 μM GSK2606414 group: $^{\#}P<0.05$. Representative images of the normal larval morphology
868 (*iii*) and of 10 μM GSK2606414- induced lordosis (*iv,* blue arrow). (**B**) Tail-trunk angle
869 measurement representation (blue line) and quantification at 76 hpf. (**C**) Body length
870 measurement representation (blue line) and quantification at 76 hpf. Data in percentage of
871 control body length. $n = 15$ larva. One-Way ANOVA with Dunnett's post-hoc test: $^{*}P < 0.05$
872 vs 0 μM GSK2606414. (**D**) Effect of muscle relaxant d-tubocurarine (dTC, 0.03–3 mM) on
873 touch-evoked escape response (TEER) after (*i*) head or (*ii*) tail touches at 76 hpf . n= 3
874 independent experiments. Data in percentage of total touches. One-Way ANOVA with
875 Dunnett's post-hoc test: $^{*}P < 0.05$ vs 0 mM dTC. Grey band indicates the mean ± SEM of each
876 parameter in control larva. (**E**) Contribution of muscle contraction for morphological defects
877 at 76 hpf. Representative images of (*i*) control larvae and larvae treated with (*ii*) 3 mM dTC,
878 (*iii*) 10 μM GSK2606414 or (*iv*) 3 mM dTC in combination with 10 μM GSK2606414. Lordosis
879 (arrow). (*v*) Quantification of larvae presenting morphological defects upon 10 μM

880 GSK2606414 and 3 mM dTC treatment. N= 3 independent experiments. Data in percentage of
881 live larvae at 4 hpf. One-Way ANOVA with Sidak's post-hoc test: *$P < 0.05$ vs control.
882
883 **Fig. 4** PERK inhibition delays endocrine pancreas development. **(A)** representative images of
884 normal pancreas development in Tg(*ins:GFP, sst:mCherry*) and Tg(*ins:GFP, ela:mCherry*)
885 zebrafish. (**B)** Schematic representation of GSK2606414 treatment approaches. The area
886 labelled with (**C**) *ins:GFP*, (**D**) *sst:mCherry* or (**E**) *ela:mCherry* was used to track the
887 development of pancreatic endocrine β-cells and δ-cells, and exocrine cells, respectively.
888 Larvae were treated with 10 µM GSK2606414 from (*i*) 4 hpf until 28, 76 or 148 hpf, or from
889 (*ii*) 76 hpf to 148 hpf. Representative images of GFP and mCherry in each timepoint are located
890 under the respective condition. n = 4–33 larvae. Data are expressed as percentage of control.
891 T-test vs. control: *$P < 0.05$.
892
893 **Fig. 5** PERK inhibition induces a diabetic-like phenotype. (**A**) Representative brightfield (for
894 morphology) and fluorescence (for MitoTracker Deep Red and 2-NBDglucose) images of live
895 zebrafish treated with (*i*) 0 µM or (*ii*) 10 µM GSK2606414 from 4 to 76 hpf Image entitled
896 "neuromasts" is a greyscale version of the MitoTracker image with 2-NBDglucose and
897 Mitotracker positive neuromasts circled in yellow and MitoTracker-only positive neuromasts
898 circled in red. (**B**) Quantification of posterior (white) and anterior lateral line neuromasts
899 labelled with 2-NBDglucose according to 2017_Stengel_
900 CompBiochemPhysiolCToxicolPharmacol . n = 9–12 larvae. *T*-test vs control: *$P < 0.05$.
901
902 **Fig. 6** PERK inhibition decreases neuro-motor responses and impairs muscle integrity. (**A**)
903 Evaluation of spontaneous zebrafish movement – tail coilings. (*i*) Representative images of a
904 time-lapse acquired during a tail coiling movement; a white line representing notochord

905 highlights zebrafish movement. (*ii*) Quantification of tail coilings in larvae treated with
906 increasing concentrations of GSK2606414 at 28 hpf. *n*= 23 – 26 larvae. Data in percentage of
907 number of tail coilings in control larvae. (**B**) Quantification of touch-evoked escape responses
908 (TEER) after head (*i*) or tail (*ii*) touches at 76 hpf. N= 13-114 larva. Data in percentage of
909 number of total touches. Grey band indicates the mean ± SEM of each parameter in control
910 larva (**C**) Evaluation of muscular integrity using light birefringence. (*i*) Muscle birefringence
911 as polarized light goes through zebrafish muscle sarcomeres; (*ii*) Representative images of
912 muscle birefringence in zebrafish larvae at 76 hpf. (*iii*) Quantification of zebrafish
913 birefringence intensity. *n*=15 larvae. Data in percentage of birefringence intensity in control
914 larva. One-Way ANOVA with Dunnett's post-hoc: **P* < 0.05 vs 0 µM GSK2606414. Grey
915 band indicates the mean ± SEM of each parameter in control larva.
916
917 **Fig. 7** PERK inhibition induces morphological and functional cardiac defects. (**A**) Cardiac
918 oedema in live zebrafish larvae treated with increasing concentrations of GSK2606414 at 28,
919 52 and 76 hpf. (*i*) Quantification of live larvae with cardiac oedema through time. *n*=5
920 independent experiments. Data in percentage of live larva at 4 hpf. A significant interaction (*P*
921 < 0.05) between concentration and time was found and Sidak post-hoc test was performed to
922 compare the percentage of larvae with cardiac oedema between different drug concentrations
923 within each time point: **P*<0.05 vs 0 µM GSK2606414. Representative images of zebrafish
924 larvae at (*ii*) 28 hpf and (*iii*)76 hpf treated with 0 (control) or 10 µM GSK2606414. Cardiac
925 oedema (blue arrow). (**B**) Monitoring functional abnormalities in zebrafish heart at 76 hpf. (*i*)
926 Quantification of zebrafish heartbeat when treated with increasing GSK concentrations at
927 76hpf. *n*= 13 – 116 larvae. Grey line indicates the mean ± SEM heartbeat in control larva. Data
928 in heartbeats per minute (bpm). One-Way ANOVA with Dunnett's post-hoc: **P* < 0.05 vs 0
929 µM GSK2606414. (*ii*) Representative images of the structure of zebrafish heart and plots of

930 atrio-ventricular coordination in control and 10 μM GSK2606414 treated larvae (a: atrium –

931 red; v: ventricle - blue).

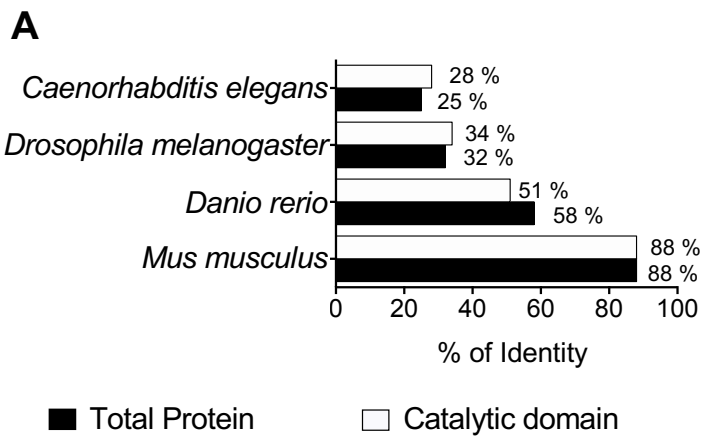

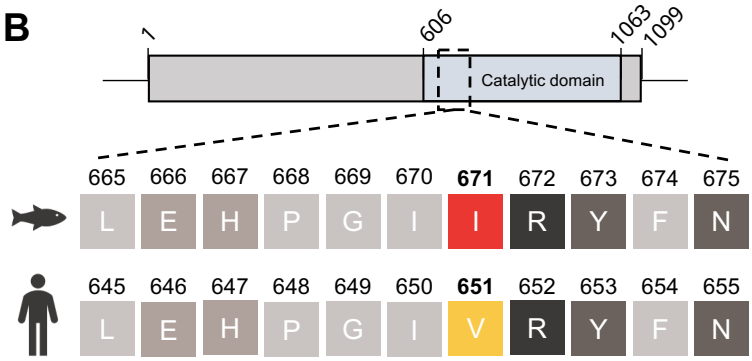

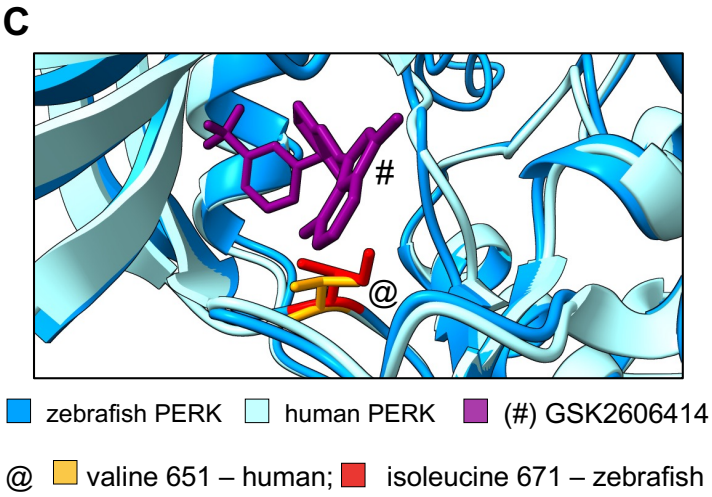

D

Metric		Value	Reference values for similarity		Ref
RMSD	Active site	0.371Å	High	0-1 Å	1
	Total protein	0.868 Å	Moderate	1-3 Å	
			Low	> 3 Å	
Ramachandran outliers		10.21%	High	0%	2

RMSD, Root Mean Square Deviation

[1] Carugo O. et al., **2001**, *Protein Science*, doi: 10.1110/ps.690101.

[2] Chen B. et al, **2009**, *Acta Crystallographica*, doi:10.1107/S0907444909042073.

Figure 1

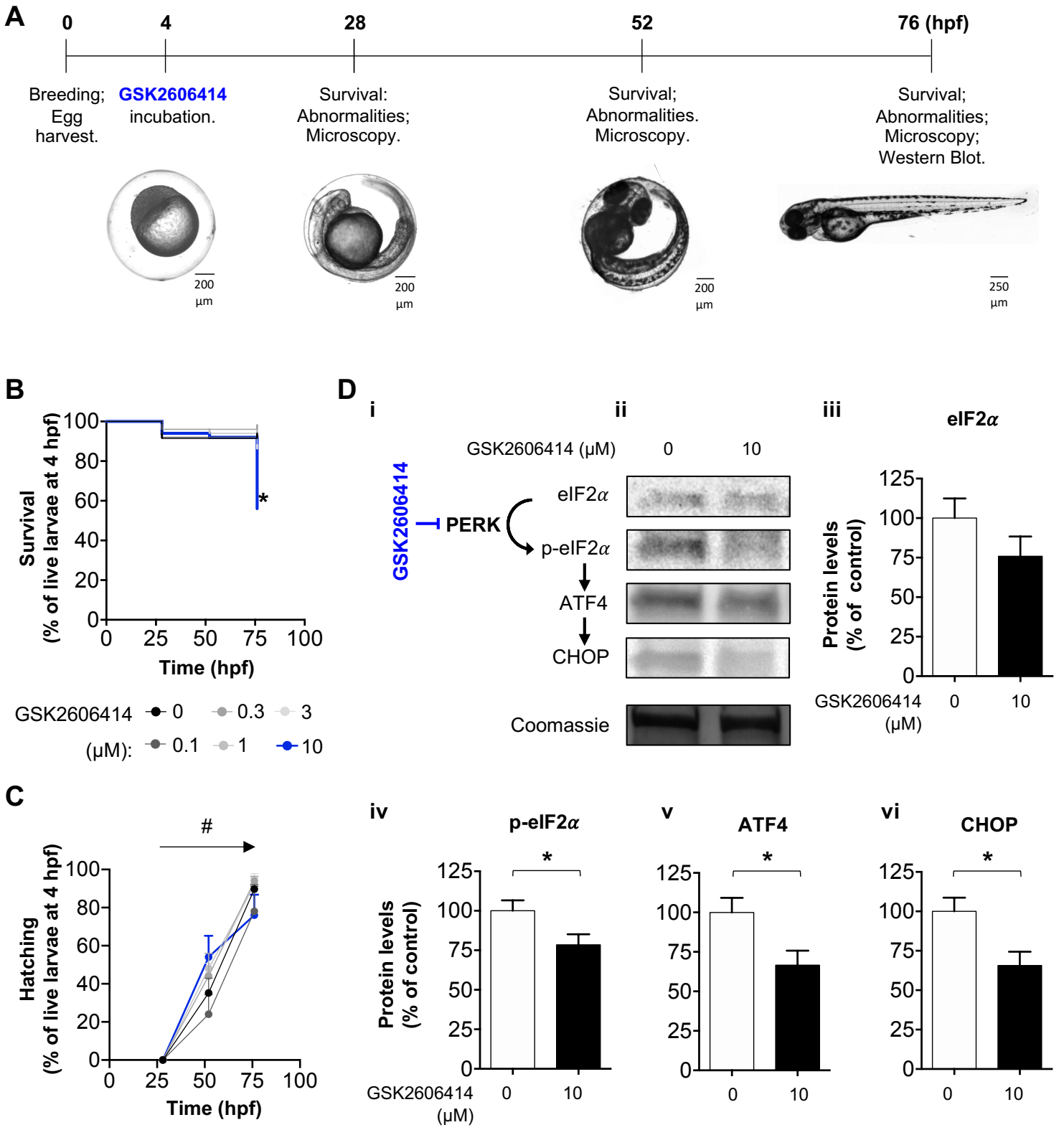
A
0
4
28
52
76 (hpf)
Breeding; Egg harvest.
GSK2606414 incubation.
Survival: Abnormalities; Microscopy.
Survival; Abnormalities. Microscopy.
Survival; Abnormalities; Microscopy; Western Blot.
200 µm
200 µm
200 µm
250 µm
B
Survival (% of live larvae at 4 hpf)
Time (hpf)
GSK2606414 (µM): 0 0.3 3 0.1 1 10
C
Hatching (% of live larvae at 4 hpf)
Time (hpf)
#
D
i
ii
iii
GSK2606414 (µM) 0 10
GSK2606414
PERK
eIF2α
p-eIF2α
ATF4
CHOP
Coomassie
eIF2α
Protein levels (% of control)
GSK2606414 (µM) 0 10
iv
p-eIF2α
v
ATF4
vi
CHOP
Protein levels (% of control)
GSK2606414 (µM) 0 10

Figure 2

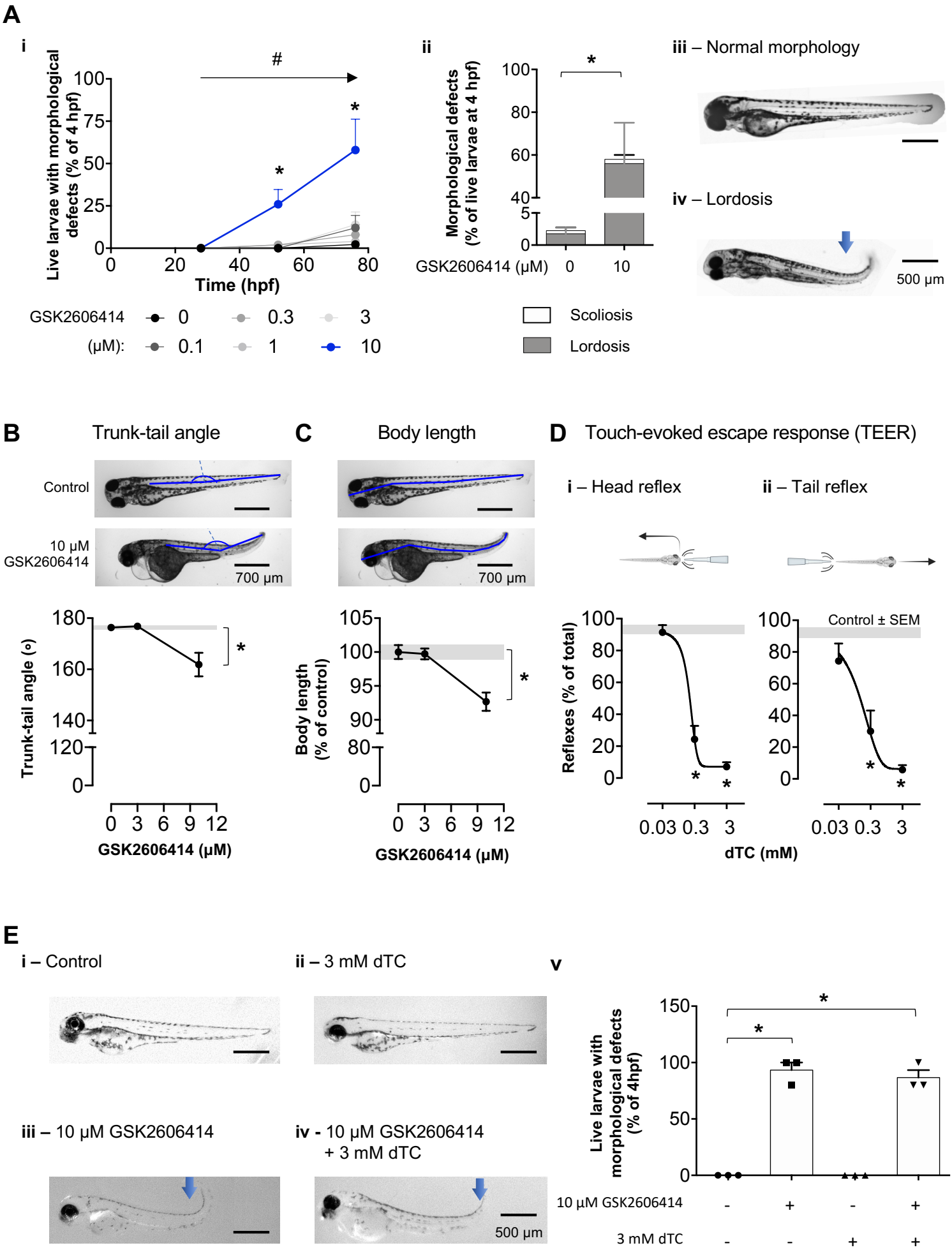
A
i
Live larvae with morphological defects (% of 4 hpf)
Time (hpf)
GSK2606414 (µM): 0 0.1 0.3 1 3 10
ii
Morphological defects (% of live larvae at 4 hpf)
GSK2606414 (µM) 0 10
Scoliosis
Lordosis
iii – Normal morphology
iv – Lordosis
500 µm
B
Trunk-tail angle
Control
10 µM GSK2606414
700 µm
Trunk-tail angle (°)
GSK2606414 (µM)
C
Body length
700 µm
Body length (% of control)
GSK2606414 (µM)
D
Touch-evoked escape response (TEER)
i – Head reflex
ii – Tail reflex
Reflexes (% of total)
Control ± SEM
dTC (mM)
E
i – Control
ii – 3 mM dTC
iii – 10 µM GSK2606414
iv - 10 µM GSK2606414 + 3 mM dTC
500 µm
v
Live larvae with morphological defects (% of 4hpf)
10 µM GSK2606414
3 mM dTC

Figure 3

Figure 4

A

i – 28 hpf

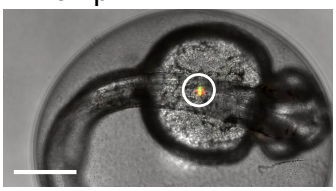

ins:GFP
sst:mCherry

ii – 76 hpf

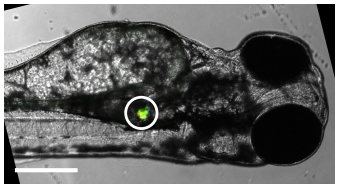

ins:GFP
sst:mCherry

iii – 148 hpf

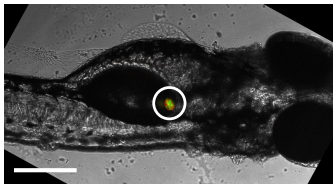

ins:GFP
sst:mCherry

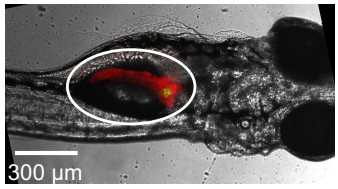

ins:GFP
ela:mCherry

B

i – **Start**: 4 hpf

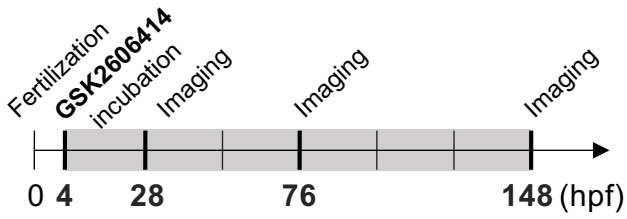

ii – **Start**: 76 hpf

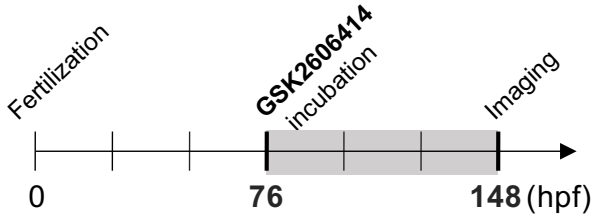

C – ***ins:GFP***

i – **Start**: 4 hpf → 28 hpf | 76 hpf | 148 hpf

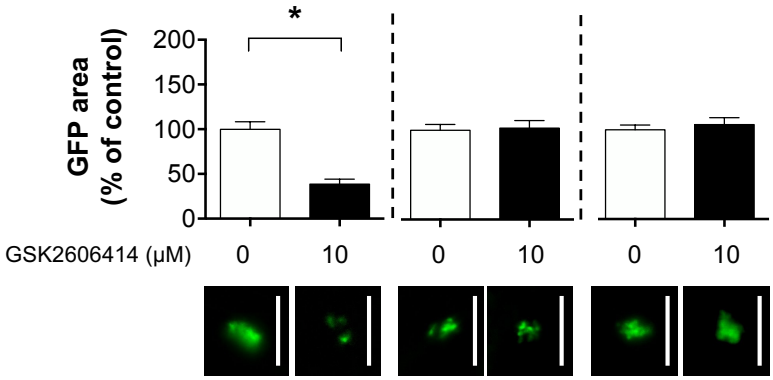

ii – **Start** 76 hpf → 148 hpf

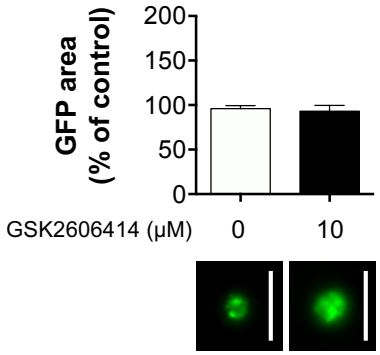

D – ***sst:mCherry***

i – **Start**: 4 hpf → 28 hpf | 76 hpf | 148 hpf

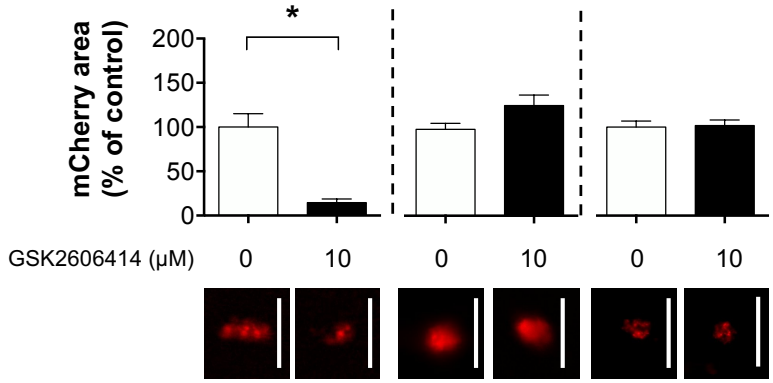

ii – **Start** 76 hpf → 148 hpf

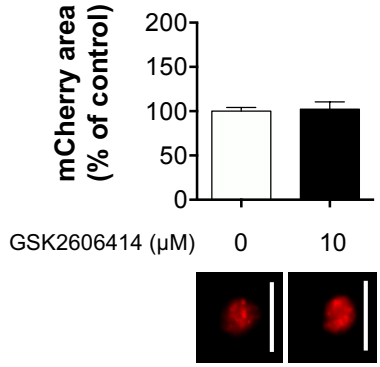

E – ***ela:mCherry***

i – **Start**: 4 hpf → 148 hpf

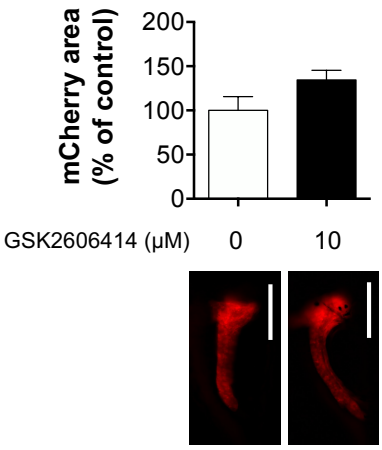

ii – **Start** 76 hpf → 148 hpf

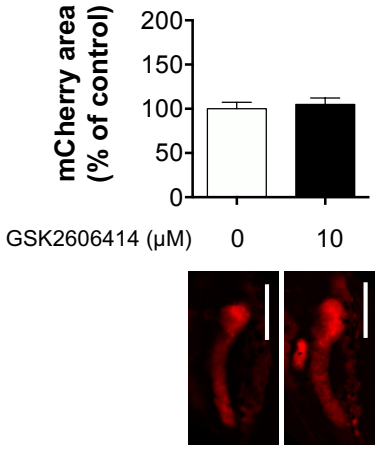

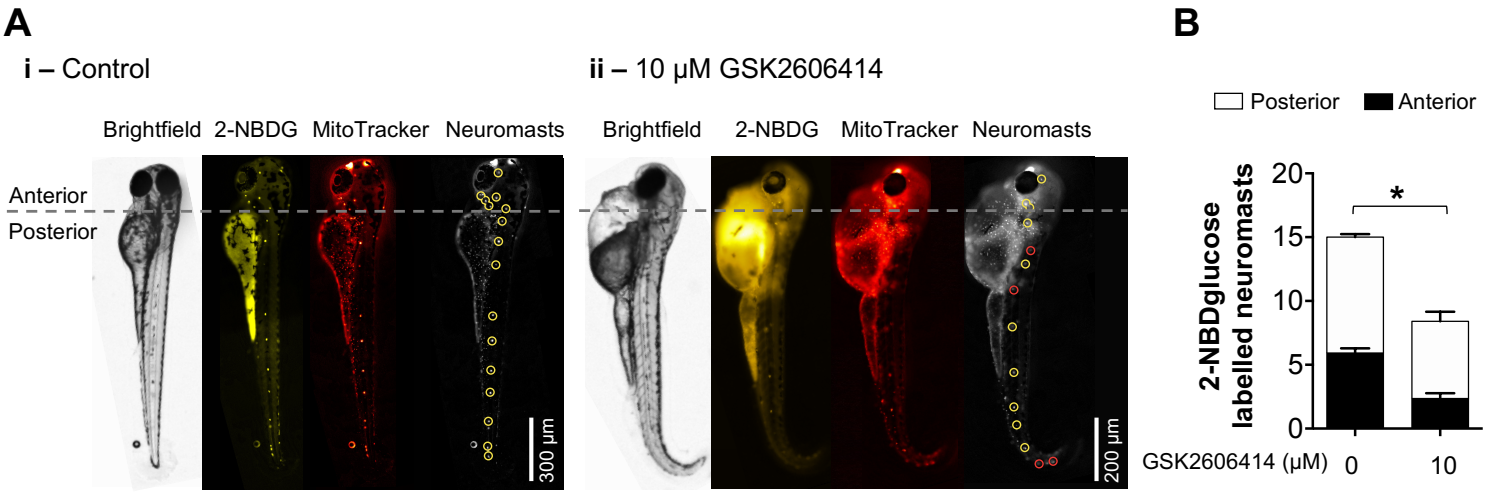
A
i – Control
ii – 10 µM GSK2606414
Brightfield
2-NBDG
MitoTracker
Neuromasts
Brightfield
2-NBDG
MitoTracker
Neuromasts
Anterior
Posterior
300 µm
200 µm
B
Posterior
Anterior
2-NBDglucose labelled neuromasts
20
15
10
5
0
*
GSK2606414 (µM)
0
10

Figure 5

A Tail coilings (28 hpf)

i

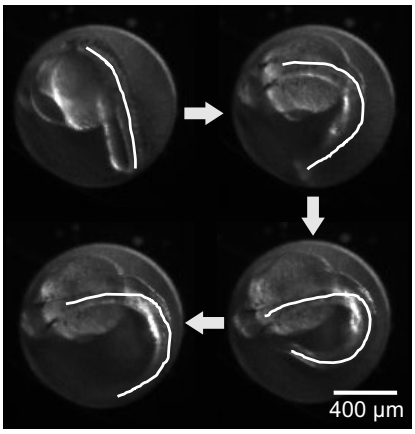

ii

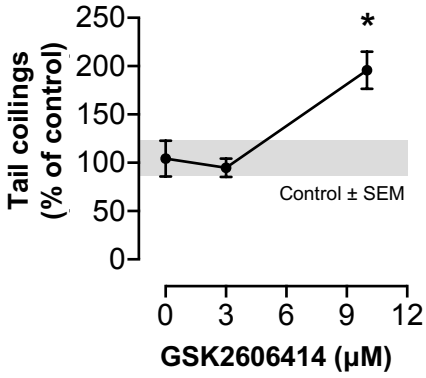

B Touch-evoked escape response (TEER)

i

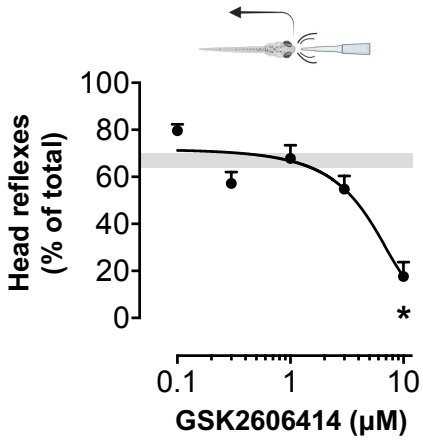

ii

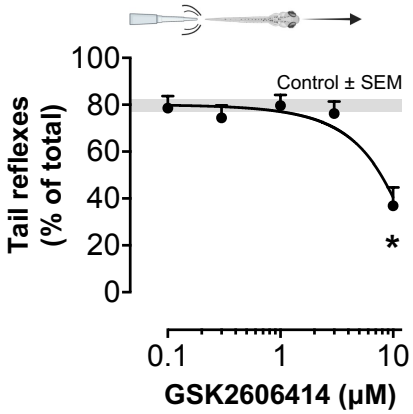

C Birrefringence assay

i

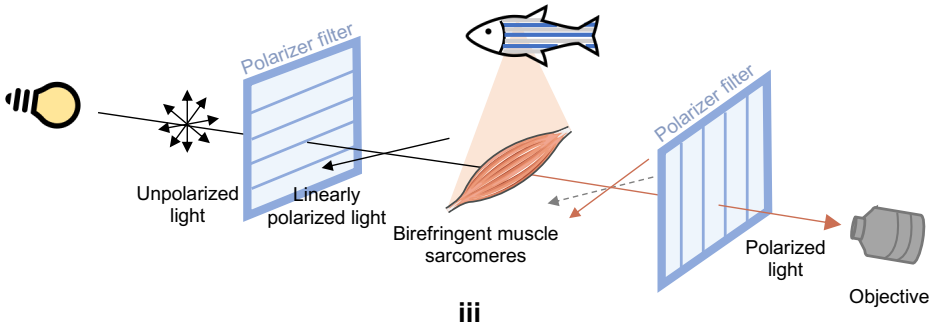

ii

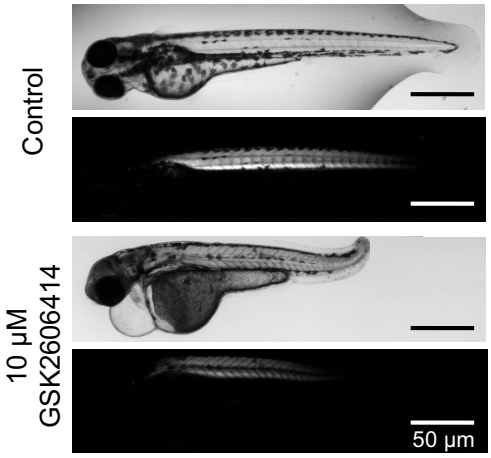

iii

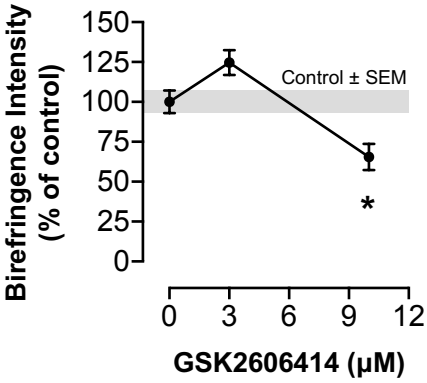

Figure 6

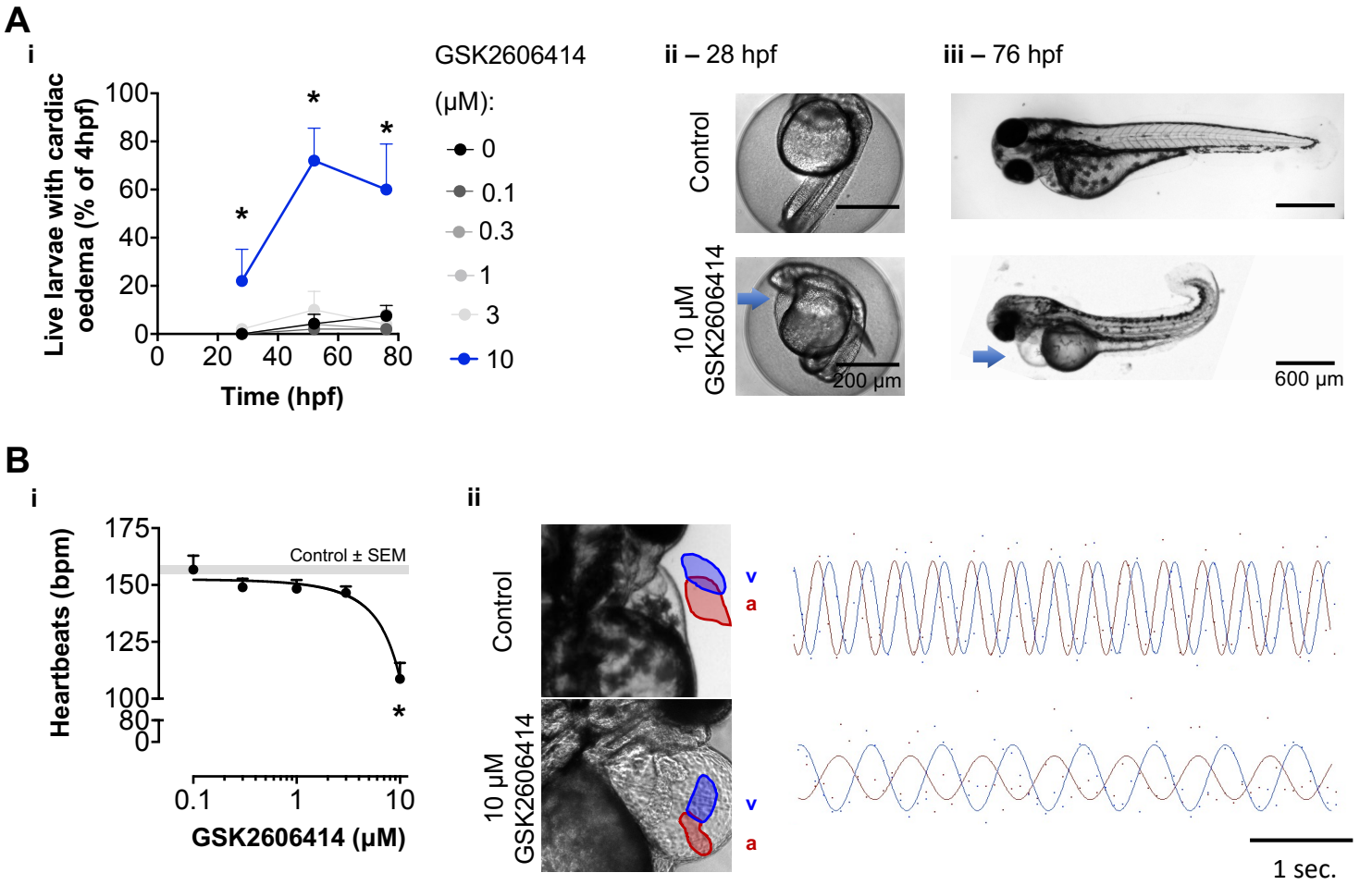
A
i
Live larvae with cardiac oedema (% of 4hpf)
100
80
60
40
20
0
0
20
40
60
80
Time (hpf)
*
*
*
GSK2606414 (μM):
0
0.1
0.3
1
3
10
ii – 28 hpf
iii – 76 hpf
Control
10 μM GSK2606414
200 μm
600 μm
B
i
Heartbeats (bpm)
175
150
125
100
80
0
Control ± SEM
*
0.1
1
10
GSK2606414 (μM)
ii
Control
10 μM GSK2606414
v
a
v
a
1 sec.

Figure 7